IMPLEMENTATION AND APPLICATION OF SAPRC07 AND MCM MECHANISMS IN THE COMMUNITY MULTI-SCALE AIR QUALITY MODEL

A Thesis

by

JINGYI LI

Submitted to the Office of Graduate Studies of
Texas A&M University
in partial fulfillment of the requirements for the degree of

MASTER OF SCIENCE

December 2010

Major Subject: Civil Engineering

Implementation and Application of SAPRC07 and MCM Mechanisms in the

Community Multi-Scale Air Quality Model

IMPLEMENTATION AND APPLICATION OF SAPRC07 AND MCM IN THE COMMUNITY MULTI-SCALE AIR QUALITY MODEL

A Thesis

by

JINGYI LI

Submitted to the Office of Graduate Studies of
Texas A&M University
in partial fulfillment of the requirements for the degree of

MASTER OF SCIENCE

Approved by:

Chair of Committee,	Qi Ying
Committee Members,	Bryan Boulanger
	Renyi Zhang
Head of Department,	John Niedzwecki

December 2010

Major Subject: Civil Engineering

ABSTRACT

Implementation and Application of SAPRC07 and MCM Mechanisms in the Multi-scale Community Air Quality Model.

(December 2010)

Jingyi Li, B.S., Tianjin University, China

Chair of Advisory Committee: Dr. Ying Qi

A photochemical mechanism is a very important component of an air quality model, which simulates the change of pollutant concentrations due to chemical reactions in the air. The accuracy of model prediction is directly impacted by the photochemical mechanism. In this study, two state-of-the-science photochemical mechanisms, SAPRC07 and Master Chemical Mechanism (MCM) v3.1, were implemented in the Community Multi-scale Air Quality Model (CMAQ) version 4.6 developed by the US EPA to study a high ozone (O_3) episode during the 2000 Texas Air Quality Study (TexAQS) from August 16, 2000 to September 7, 2000.

Predicted O_3 concentrations by S07C are lower than those of S99 with a maximum difference as high as 20%. The two mechanisms also show significant differences in the predicted OH, PAN, HCHO and HNO_3 concentrations. Although the two mechanisms predict different ozone concentrations, the relative response factors (RRFs) of O_3 at rural, urban and industrial sites under emission controls of anthropogenic NOx and VOC by factors 0.6 – 1.4 predicted by the two mechanisms are very similar. Predicted O_3

concentrations by MCM are similar to those of SAPRC07. The MCM predicted total VOC OH reactivity is similar to the SAPRC07 predictions at a suburban site where biogenic emissions dominate the OH reactivity and is slightly lower than the SAPRC07 predictions at an industrial site where anthropogenic emissions dominate. Besides, the predicted 1-hr and 24-hr average concentrations of major O_3 precursor VOCs by MCM show under predictions of alkanes and alkenes by a factor of 2-5, 6 for ethane and 8.5 for propane. Major aromatic compounds generally agree better with observations, although benzene is under-predicted by 80%. Species specific emission adjustment factors can be derived from these direct comparisons to improve emission inventories in future studies. At the Clinton Drive site, most of the under-predictions occur in the afternoon when industrial facilities are in the immediate upwind direction and the missing industrial emissions are likely evaporative sources whose emission rates are temperature dependent.

DEDICATION

I would like to dedicate this work to my mother, father and my dear grandma who has passed away. Their encouragement and support drive me to overcome difficulties in life and study, without which I could not be where I am now.

ACKNOWLEDGEMENTS

I would like to thank my advisor Dr. Qi Ying for his patient teaching and valuable guidance on my research, without which I could not achieve such progress today. I would also like to express my gratefulness on my committee chair members, Dr. Bryan Boulanger and Dr. Renyi Zhang for their support and encouragement during my graduate study. I feel honored to have them in my thesis committee.

In addition, I would like to thank Dr. William P.L. Carter for providing the SAPRC07 photochemical mechanism, and Mark Estes of the Texas Commission of Environmental Quality (TCEQ) for providing us the GC-ITMS and GC-FID data.

Last, but not the least, I would like to thank people in our group, Sri Harsha Kota, Hongliang Zhang, Sajjad Ali, and Gang Chen for their unselfish help when I met difficulties with my research and study.

TABLE OF CONTENTS

LIST OF FIGURES

Page

Page

Page

LIST OF TABLES

Page

1. INTRODUCTION

Making accurate assessment of the effectiveness of emission controls in reducing photochemical air pollution is important for policy makers to determine optimal emission control strategies to better protect human health and the environment. Air quality models are widely used to study air pollution and to evaluate various emission control scenarios by simulating the physical and chemical processes related to air pollutant formation and transport in the atmosphere. One of the major components of an air quality model is the photochemical mechanism that describes photochemical transformation of natural and anthropogenic emissions of nitrogen oxides (NOx) and volatile organic compounds (VOCs) in the atmosphere that forms secondary pollutants such as ozone (O_3), intermediate oxidation products and secondary organic aerosol (SOA).

Several different photochemical mechanisms are currently being used in various urban and regional air quality models, including the Carbon Bond (CB) mechanisms (Gery et al., 1989; Yarwood et al., 2005), the RACM mechanism (Stockwell et al., 1997), the Master Chemical Mechanism (MCM) (Jenkin et al., 1997; Jenkin et al., 2003; Saunders et al., 2003), the Caltech Atmospheric Chemical Mechanism (CACM) (Griffin et al., 2005) and the SAPRC mechanisms (Carter, 1990; Carter, 2000; Carter, 2010). These photochemical mechanisms differ in the level of condensed representations of volatile organic compounds and organic radicals and the reactions among the

---

This thesis follows the style of Atmospheric Environment.

compounds and radicals, the completeness of the inorganic part of the gas phase chemistry and the reaction rate coefficients. These differences could lead to variations in the predicted O_3 and other pollutant concentrations.

The SAPRC photochemical mechanisms are one of the most widely used photochemical mechanism families for both regulatory and research applications in the United States (Carter, 1994; Czader et al., 2008). It has been extensively compared with other photochemical mechanisms. For example, Ying et al. (Ying et al., 2007) found that peak O_3 concentrations predicted by the CACM mechanism is approximately xx% higher than the SAPRC-90 mechanism in the South Coast Air Basin (SoCAB) in California. Jimenez et al. (2003) compared commonly used photochemical mechanisms, including CB 4, RACM, SAPRC-99 (S99) and CACM, in a box model. It was found that the O_3 predictions are quite similar but the predicted oxidation products such as HNO_3 and PAN (peroxylaceylnitrate) are significantly different among the mechanisms. Byun (2002) and Faraji et al.(2008) compared the CB4 with S99 in Southeast Texas and noticed that S99 predicted higher O_3 by as much as 50 ppb.

The S99 mechanism, which was released in 1999 and has been actively used for more than 10 years, has been updated recently to SAPRC-07 (S07) to incorporate the recent developments in atmospheric chemistry of VOCs to O_3 formation (Carter, 2010). Several studies have been conducted to evaluate the S07 mechanisms by comparing with existing mechanisms, including S99, RACM and MCM in box model setting for incremental O_3 reactivity (Derwent et al. 2008) and chamber data (Azzi et al., 2008). The

S07 mechanism has been determined to represent the current state of science (Stockwell, 2009).

Initial applications of the S07 mechanism in 3D Eulerian air quality models show quite significant differences of the predicted O_3 concentrations between S99 and S07 in California (Cai et al., 2010). However, detailed comparison of S99 and S07 has not been reported for other parts of the country. In addition, the implications of the differences in the development of emission control strategies have not been studied. For example, one of the applications of the air quality model in regulatory settings is to determine the relative response factor (RRF), which is the ratio of the predicted 8-hour max O_3 concentration near a monitoring station under a hypothetical future year emission scenario to the base case result. The RRF is applied to scale the 8-hour O_3 design value (DV) to calculate the DV for the future year, which is the basis for compliance determination (EPA, 2007). It is not clear whether the two mechanisms will predict similar RRFs or not under identical emission control scenarios.

The Houston-Galveston Bay (HGB) and Beaumont-Port Arthur (BPA) areas in Southeast Texas are in violation of the NAAQS 8-hour O_3 standard (EPA, 2004). Emission sources and meteorology conditions that lead to high O_3 concentrations are different than those in the SoCAB and Central Valley of California. Large amounts of highly reactive VOCs emitted from petrochemical industrial sources combining with significant amount of urban emissions of NOx and VOCs lead to high O_3 formation rate. Alteration of land- and sea-breeze with relatively slow wind speed leads to accumulation of pollutants (TCEQ, 2002). These differences in emissions and meteorology may lead

to differences between S99 and S07 that are not expected from simulations for the SoCAB.

Current emission inventories include many hundreds of types of volatile organic compounds (VOCs) (Carter, 2004), each of which react at different rates and mechanisms and form a large number of oxidation products that influence the formation of O_3 and other secondary pollutants (NRC, 1991). In order to better understand the underlying causes of O_3 pollution and to design effective emission reduction strategies, air quality monitoring efforts in non-attainment areas have been focused on measuring the concentrations of important VOC O_3 precursors along with O_3, nitrogen oxides (NO_x) and meteorology conditions, among other parameters. A large amount of chemically speciated VOC data have been collected using canister sampling/gas chromatography at stations throughout the country. In recent years, automatic gas chromatography instruments become more widely used for hourly speciated VOC data.

One of the applications of these detailed VOC data is to assess the accuracy of the existing emission inventories. Previous studies utilized receptor-oriented methods to determine the contributions of different sources to the observed concentrations (Buzcu and Fraser, 2006; Henry et al., 1994; Zhao et al., 2004). Source contributions at monitoring sites were compared with reported emission rates to identify potential biases in the emission inventory (Brown et al., 2004; Buzcu-Guven and Fraser, 2008). Although the receptor-oriented techniques are useful, chemical reactions of the VOCs are often difficult to account for, limiting the analysis on night time samples (Watson et al., 2001). The accuracy of these assessments is difficult to evaluate directly. Instead, the

properness of the proposed adjustments to the emission inventory is often indirectly tested by evaluating the model performance on O_3 using 3D air quality models (Byun et al., 2007). An alternative and more direct method is to apply 3D air quality model to predict concentrations of individual VOC based on the emission inventory and compare the predicted concentrations with observations so that problems in the emission inventory can be directly identified and the effectiveness of proposed emission inventory updates can be evaluated.

Traditional 3D air quality models use condensed photochemical mechanisms that group large amounts of VOCs and their intermediate oxidation products into a few model species based on their molecular structures or reactivity (Carter, 1994; Carter, 2010 (quotation is wrong); Dodge, 2000; Gery et al., 1989). Direct comparison of observed VOCs is only possible for the species that are explicitly represented by the mechanism. Few 3D air quality modeling studies have been done to simultaneously model a large number of explicit VOC species. Harley and Cass (1995) developed the first 3D Eulerian model that explicitly tracks 53 individual organic species based on a detailed SARPC gas phase chemical mechanism (Carter, 1990) and Fraser et al. (2000) expanded the mechanism to treat 135 explicit VOCs. These models were applied to simulate individual VOC concentrations in the South Coast Air Basin (SoCAB) of California for a 3-day and a 2-day episode in August 1987 and September 1993, respectively.

Recently, a near-explicit photochemical mechanism, the Master Chemical Mechanism (MCM), was developed to represent the multi-step degradation of a large number of

primary emitted VOCs in the troposphere using approximately 5,000 explicit species and 13,500 reactions (Bloss et al., 2005; Jenkin et al., 1997; Jenkin et al., 2003; Saunders et al., 2003). The detailed mechanism allows predictions of a large number of primary organic compounds, organic radicals and secondary products using a set of protocols based on existing knowledge of major reaction pathways, branching ratios and reaction products (Jenkin et al., 1997; Jenkin et al., 2003). The advantage of the MCM to the mechanisms used in previous individual VOC simulation studies is that the detailed chemical composition of SOA can also be predicted by partitioning the semi-volatile organic compounds explicitly between the gas and particle phases (Johnson et al., 2004, 2005; Johnson et al., 2006a; Johnson et al., 2006b). The MCM mechanism has been partially tested using chamber experiments and field observations (for example, see (Pinho et al., 2006, 2007; Pinho et al., 2005)), and compared with other chamber validated photochemical mechanisms using box model and trajectory model simulations (Carslaw et al., 1999; Emmerson et al., 2004; Liang and Jacobson, 2000). More recently, a version of the MCM has been implemented in a multi-scale 3D coupled meteorology/air quality model and preliminary applications of the model for a limited 3 day simulation for the SoCAB was reported for gas phase species (Jacobson and Ginnebaugh, 2010).

The objective of this study is to 1) compare the S07 with the S99 mechanism in the Community Air Quality Model (CMAQ) model (Byun and Schere, 2006) for a high O_3 episode in Southeast Texas to better understand the causes of the differences in O_3 predictions and responses to emission controls. Applying S07 in this region provides

additional test of the capability of the mechanism and comparing its performance with S99 provide further evaluation of the difference between S99 and S07. 2) implement the near-explicit MCM photochemical mechanism in CMAQ (referred to as CMAQ-MCM hereafter) for predictions of detailed spatial distribution of gas phase organic compounds and to apply the CMAQ-MCM to a representative air quality episode in the southeast Texas to evaluate the biases in the predicted VOC concentrations. It is the first study to compare a large number of 1-hr resolution VOC observations with predictions from an advanced 3D air quality model. In the long run, implementing the SAPRC07 and MCM mechanisms in the widely used CMAQ modeling framework will allow this valuable tool to be used by a large potential user base for various research purposes.

2. COMPARISON OF THE SAPRC07 AND SARPC99 PHOTOCHEMICALMECHANISMS DURING A HIGH OZONE EPISODE IN TEXAS

2.1 Mechanism Description

The SAPRC series of photochemical mechanisms were initially developed in the early 1990s at the Statewide Air Pollution Research Center (SAPRC) in California and went through continuous update throughout the past two decades. Details of the S99 and S07 have been well documented elsewhere (Carter, 2000; Carter, 2010) and only a brief summary is provided.

The SAPRC mechanisms are designed in a modular configuration: a base case mechanism and swappable mechanisms for emitted VOCs with different levels of complexity. The base case mechanism involves the reactions of inorganic species, common organic products and their intermediate radical precursors. The mechanisms for emitted VOC species have separate versions with significant differences in the level of complexity. The detailed versions of the S99 and S07 VOC mechanisms use separate representations of the reactions for 550 and 750 VOC categories, respectively, mostly for calculating VOC reactivity scales in box model settings. The versions for 3D air quality model applications use 10 lumped model species to represent the reactions of majorities of the emitted VOCs. These versions are often referred to as the “standard” version of the SAPRC mechanisms. In additional to the updates in the photolysis data and reaction

rate constants and the inclusion of chlorine reactions, major updates in the S07 are peroxy radical representations and aromatic mechanisms. The S07 mechanism is capable of predicting the change of the products from peroxy + peroxy radical reactions under different NOx levels. Initial ring fragmentation reactions of aromatics are simplified and less parameterized to give better simulation of available reactivity data. In addition, two new higher hydroperoxides (R6OOH and RAOOH) are added which have different OH reactivates and SOA formation potentials.

There are several different versions of S07 designed for 3D airshed models. The standard versions including S07A (use condensed peroxy radical operator representation as used in SAPRC-99), S07B (use chemical operators for peroxy radicals to reduce the number of reactions, not compatible with CMAQ) and S07C (same as S07B but compatible with CMAQ), and the versions with additional model species to represent selected air toxic species explicitly. In our study, the standard S07C is applied because it is the most expanded mechanism compatible with CMAQ model.

2.2 Model Application

The Community Multi-scale Air Quality model version 4.6 (CMAQ v4.6) is used as the host model to implement the most recent version of the S07C mechanism from the SAPRC website (http://www.engr.ucr.edu/~carter/SAPRC/files.htm; Last update of the S07C mechanism file SAPRC07C.MEC is January 25, 2010). Quantum yield and absorption cross section data for S07C are also downloaded from the SAPRC

mechanism website (file PHF.ZIP, last updated October 29, 2008). The S99 mechanism is already included in CMAQ v4.6. In this study, both aerosol and aqueous phase reactions are not considered for a direct comparison of the gas phase mechanisms. Both mechanisms are solved using the SMVGEAR solver (Jacobson and Turco, 1994) included in the CMAQ distribution.

The CMAQ models are applied to study a three-week O_3 episode (August 16 to September 6, 2000) during the 2000 Texas Air Quality Study (TexAQS 2000) using a three-level nested domain (Figure 2.1). Details of the domain setup and preparation of initial and boundary conditions have been described in detailed in Ying and Krishnan (Ying and Krishnan, 2010) and is briefly summarized below. The coarse domain is for the eastern United States with 36 km horizontal resolution. The 12km inner domain covers the eastern Texas and surrounding states. The HGB and BPA areas in Southeast Texas are modeled with a 4 km horizontal resolution domain (referred to as the 4 km domain hereafter). In all the three CMAQ domains, the vertical extent of the model is divided into 14 layers. The first layer thickness is approximately 42 m. The meteorology simulation results for the episode are provided by TCEQ and are processed using the Meteorology-Chemistry Interface Processor (MCIP) to generate inputs for the CMAQ model.

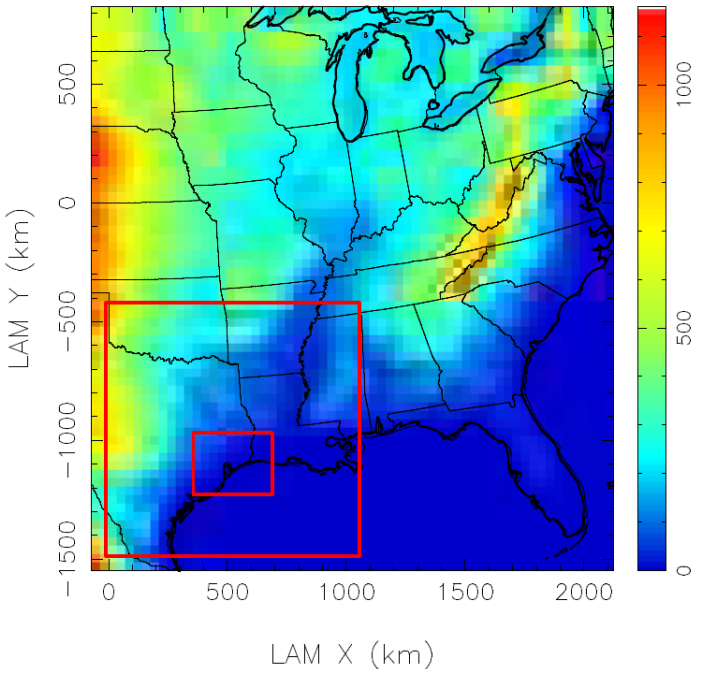

Figure 2.1 Modeling domains used in the study. Boxes show the East Texas and Southeast Texas nested domains. Colors represent surface elevation above sea level.

EPA's 2001 CAIR (Clean Air Interstate Rules) emission inventory was used to generate emission inputs for the TexAQS 2000 episode. A revised Sparse Matrix Operator Kernel Emissions (SMOKE) emission processing model (version 2.5) from US EPA was used to process the raw emission inventory to generate emissions of gases and particulate matter for each source category. Biogenic emissions were generated using the Biogenic Emissions Inventory System, Version 3 (BEIS3). VOC speciation profiles used to split total VOC emissions to S99 and S07C model species are based on the SPECIATE 3.2 database (http://www.epa.gov/ttnchie1/software/speciate/speciate32.html) and processed using the emission preprocessor program provided by Dr. William P.L. Carter (Carter, 2004) for application in the SMOKE model. The Source Classification

Code (SCC) to profile assignment file included in the CAIR emission inventory are used to determine which profile to apply for a given source.

2.3 Results and Discussions

2.3.1 Difference in predicted concentrations

Generally, S07C predicts lower O_3 concentrations than S99 in this episode. Figure 2.2(a) shows that the predicted average O_3 concentration at 11:00-12:00 CST reaches 75 ppb in downwind areas north of urban Houston. The predicted O_3 concentrations are lower than S99 by a maximum of 5 ppb, as shown in Figure 2.2(c). The difference is most significant in urban and industrial areas (the Houston Ship Channel area) where net O_3 formation rates are high (see Ying and Krishnan (2010)). In most other regions, the difference is less than 2 ppb. Near the southwest boundary, the S07C predictions are slightly higher than S99 by approximately 2 ppb. The relative difference between S99 and S07C was also calculated. In general, the difference ranges from -4% near the southwest boundary to approximately 4-6% in the Houston areas (Figure 2.2(e)). The maximum relative difference (|S99-S07|/S99) is approximately 10% in the industrial areas. Figures 2.2(b,d,f) show that the O_3 concentrations are higher in later afternoon but the difference in the predicted O_3 concentrations still ranges from -2 ppb to 4 ppb, or -4% to 10%.

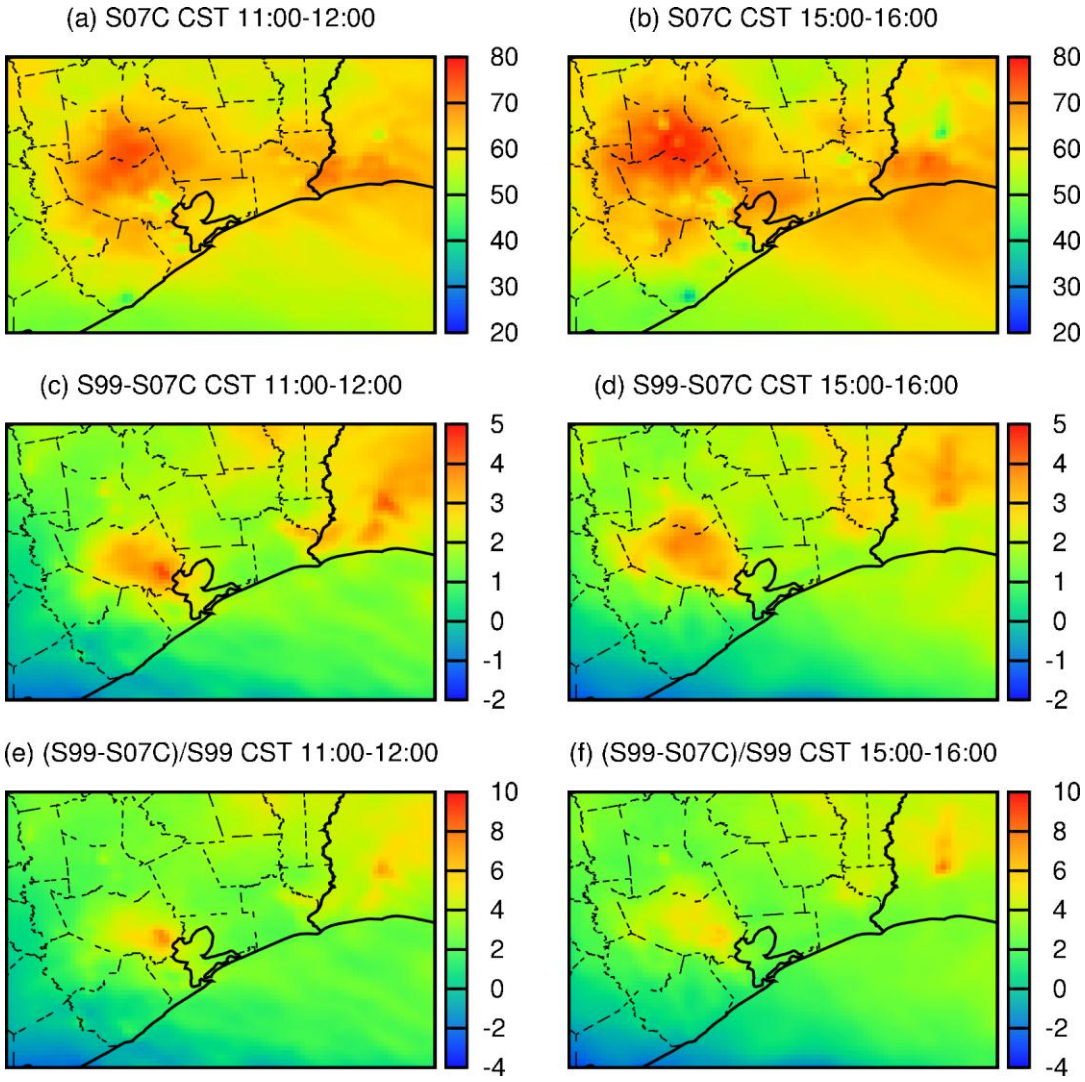

Figure 2.2 Regional distributions of O_3 concentrations predicted by SARPC99 (S99) and the difference between S99 and SARPC07 (S07) at 11:00-12:00 and 15:00-16:00 CST averaged over the entire modeling episode. Units are ppb for panels (a)-(d). The scales are different to better show the spatial distributions.

The difference in the predicted O_3 concentrations is also studied for a high O_3 day, August 31, 2000, as illustrated in Figure 2.3. On this day, off-shore flow during the day is strong and transports pollutants towards southeast. 1-hr O_3 concentration reaches as high as 160 ppb during 15:00-16:00 CST predicted by S07C. The maximum difference

between S99 and S07C reaches as high as 20 ppb during 12:00-13:00 CST in areas downwind of industrial and urban emission sources. The relative difference reaches as high as 20%.

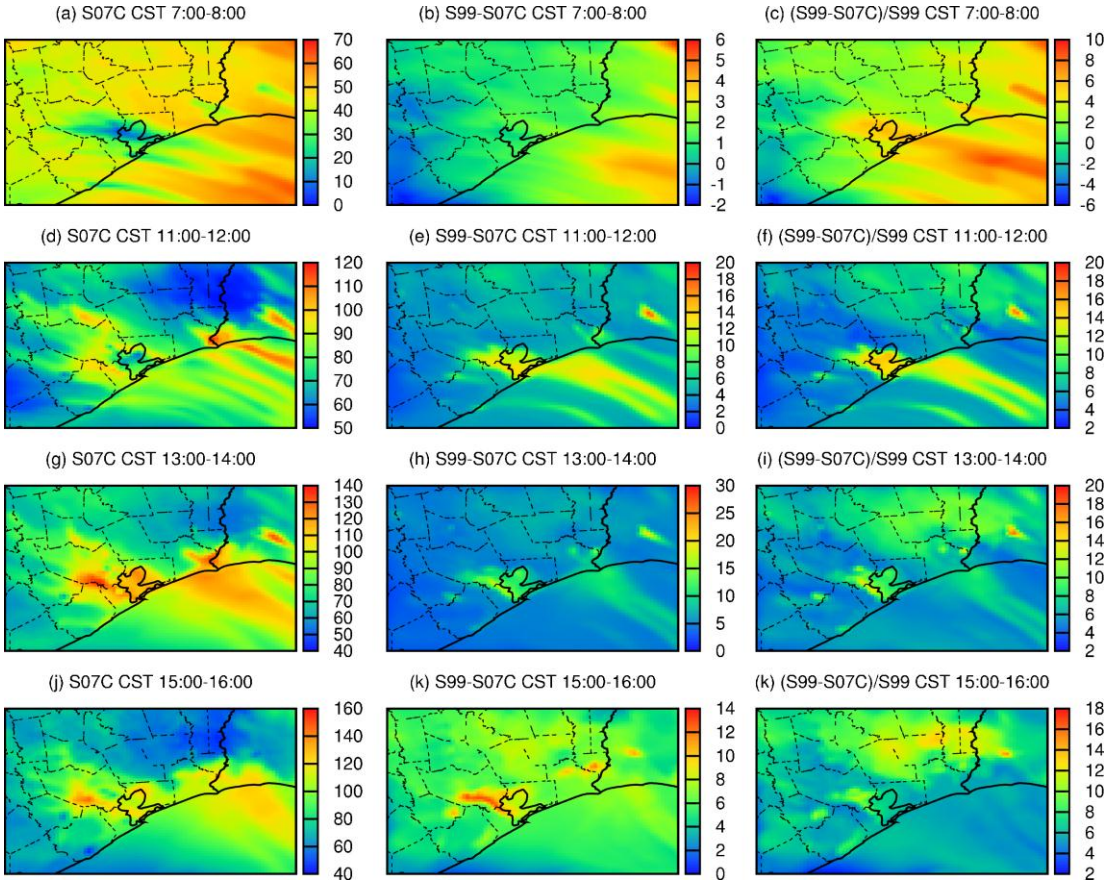

Figure 2.3 Regional distributions of O_3 concentrations predicted by S99 and the difference between S99 and S07C on August 31, 2000, a high ozone day. Units are ppb for panels in the first two columns. The scales are different to better show the spatial distributions.

Statistical model performance analysis for all the stations in the Southeast 4 km domain is presented in Table 2.1

O_3 concentrations predicted by S99 agree with observation better at almost all stations in all three criteria (mean fractional error (MFE), mean fractional bias (MFB) and accuracy of paired peak (APP), as defined below). However, the predicted O_3 concentrations are affected by not only the photochemical mechanisms but also meteorology and emission inputs. The errors caused by the uncertainties in the photochemical mechanism might be compensated by the errors in the emission inventory or meteorology. Since there are significant uncertainties in the VOC emissions, especially VOC emissions from industrial sources, and the emissions of olefin are corrected by a single scaling factor, better performance of S99 in this episode is not sufficient to judge the correctness of the mechanisms. More studies in different regions and O_3 episodes are needed to further investigate this.

Table 2.1 Statistical analysis of O_3 prediction by S99 and S07C

Site Name	Mean Fraction Error (MFE)		Mean Fractional Bias (MFB)		Accuracy of Paired Peak (APP)		Points
	S99	S07C	S99	S07C	S99	S07C	
HROC	0.31	0.30	-0.14	-0.19	-0.15	-0.19	88
HSMA	0.20	0.20	-0.05	-0.09	-0.10	-0.13	82
HCQA	0.21	0.21	-0.09	-0.13	-0.12	-0.16	97
HLAA	0.27	0.26	-0.04	-0.09	0.00	-0.05	76
HWAA	0.26	0.26	-0.10	-0.15	-0.13	-0.17	112
S40S	0.24	0.23	-0.04	-0.08	-0.15	-0.19	65
JEFC	0.21	0.21	-0.13	-0.15	-0.20	-0.22	103
C35C	0.24	0.24	-0.10	-0.16	-0.15	-0.19	74
HALC	0.25	0.28	-0.19	-0.24	-0.20	-0.24	118
TLMC	0.30	0.31	-0.18	-0.24	-0.29	-0.31	47
CLTA	0.33	0.32	-0.13	-0.20	-0.21	-0.25	27
S42S	0.14	0.17	-0.10	-0.14	-0.08	-0.12	68

Table 2.1 continued

Site Name	Mean Fraction Error (MFE)		Mean Fractional Bias (MFB)		Accuracy of Paired Peak (APP)		Points
	S99	S07C	S99	S07C	S99	S07C	
WORA	0.24	0.24	-0.12	-0.16	-0.14	-0.18	107
PAWC	0.27	0.28	-0.20	-0.23	-0.26	-0.29	128
DRPK	0.25	0.29	-0.21	-0.27	-0.25	-0.29	100
HCFA	0.31	0.30	-0.12	-0.17	-0.16	-0.20	82
GALC	0.32	0.30	-0.12	-0.15	-0.20	-0.24	66
SHWH	0.30	0.30	-0.18	-0.22	-0.13	-0.16	103
BAYP	0.24	0.26	-0.19	-0.23	-0.23	-0.26	108
HNWA	0.19	0.18	-0.04	-0.08	-0.17	-0.20	98
CONR	0.17	0.18	-0.04	-0.07	-0.18	-0.21	138
Overall	**0.25**	**0.25**	**-0.12**	**-0.16**	**-0.16**	**-0.20**	**1887**

$$MFB = \frac{2}{N}\sum_{i=1}^{N}\frac{P_i - O_i}{O_i + P_i}, MFE = \frac{2}{N}\sum_{i=1}^{N}\frac{|P_i - O_i|}{O_i + P_i}; APP = \frac{1}{N_d}\sum_{i=1}^{N_d}\frac{P_{p\_peak,i} - O_{o\_peaki}}{O_{o\_peak,i}}$$

Figure 2.4 shows the comparison of S99 and S07C on key model species at five stations that represent suburban (CONR), urban (HALC, HCFA, DRPK) and industrial (C35C) areas. Based on the slope of the linear fits, the predicted O_3 concentrations by S07C at urban sites are approximately 94% of the concentrations predicted by the S99 mechanism. At CONR, which are further away from major emission sources, the difference between the two mechanisms is only 1-2%. The differences in NO_x predictions are relatively small in urban and industrial sites, with 1-2% differences. The difference is approximately 5% in CONR. The larger differences of NO_x in suburban area are due to higher removal rate of NO_x in the S07C mechanism with OH. As the freshly emitted NO being converted to NO_2 and transported away from the emission source regions, more NO_2 is removed in the S07 mechanism due to higher NO_2 + OH reaction rates. The two mechanisms show larger differences in the predicted PAN concentrations. The difference is approximately 20-25% at urban and industrial sites and

13% at CONR. The difference is mainly caused by the additional photolysis reaction of PAN included in the S07C (in the S99, PAN does not photolyze). The S07C predicted HNO_3 concentrations are slightly higher than S99 predictions during the daytime hours. The difference becomes much more significant during night time and early morning hours as S07C predicted HNO_3 concentrations are a factor of 2 higher than S99 predictions in general. This difference is due to the addition of a homogeneous gas phase reaction of N_2O_5 with H_2O in S07C:

$$N_2O_5(g)+H_2O(g)+H_2O(g) = 2HNO_3(g);\ k=1.80\times10^{-39}\ cm^6\ molecules^{-2} \qquad (R2.1)$$

This reaction might significantly affect the amount of secondary nitrate in winter times when the meteorology conditions are more favorable for HNO_3 to partition into the particle phase (for example, in the San Joaquin Valley of California). Additional studies are needed to evaluate this modification. S99 predicts higher HCHO concentrations than S07C by approximately 12%. This difference is partly caused by the difference in the photolysis rate of HCHO, as the photolysis rate coefficients at noon time predicted by the S07C are higher than S99 by approximately 18.9% (Carter 2010). S99 also predicts higher OH radical concentrations by approximately 15-20% at urban and industrial sites and 7% difference at CONR. OH is a key species that initiate the oxidation of a large number of reactive VOC species and is regenerated during the photochemical chain reactions. The difference in the OH concentrations will be investigated in more detail in the following sections. CO, ethene and isoprene concentrations are similar between S99 and S07C. Predicted ethene and isoprene concentrations by S07C are slightly higher, probably due to lower OH concentrations.

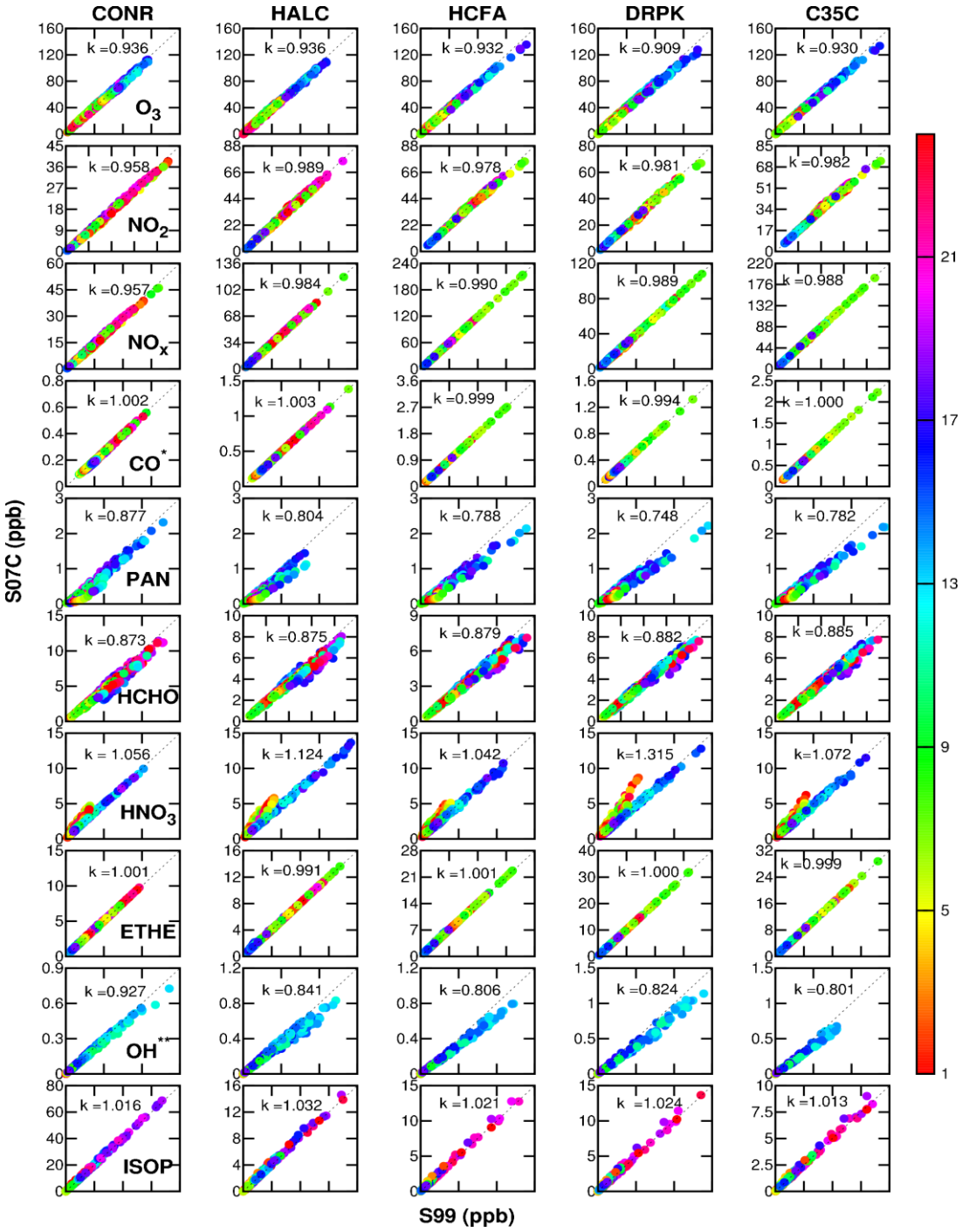

Figure 2.4 Comparison of key photochemical species. Data points are color coded by the hour of the day (CST). The slopes of linear fit between S99 and S07C (S07C=k×S99 + b) are also shown on the figure. All units are in ppb except OH, which is in units of ppt.

2.3.2 Analysis of OH and NO cycles

After initializing the VOC oxidation processes, OH can be regenerated from HO_2 + NO or HO_2 + O_3 reactions. The HO_2 is produced from organic radicals as well as from photolysis of secondary VOCs (such as such as HCHO and other higher aldehydes). Competing terminal reaction OH + NO_2 forms HNO_3, which removes the OH from the system so that the rate of OH regeneration is always less than the rate of OH reaction. The propagation factor of OH (P_{OH}) is defined as the ratio of the amount of regenerated OH to the amount of reacted OH over a time period (Jang et al., 1995). A higher propagation factor of OH means that an OH can stay in the system longer to oxidize more VOC molecules before it is removed. In addition to regeneration, "new" OH is formed from freshly emitted VOCs (mostly aldehydes) that photolysis to produce HO_2. OH from these freshly emitted VOCs is considered as "new" OH and should be subtracted from the overall OH generated from HO_2, as they are not "regenerated". OH from H_2O + $O(^1D)$ reaction is also considered as "new" OH.

In this study, freshly emitted aldehydes and secondary aldehydes generated from parent VOCs are tracked separately using tagged reactive species approach (Ying and Krishnan, 2010). As an example, the freshly emitted formaldehyde in the mechanisms is tracked using species HCHO, while the secondary formaldehyde produced by other VOCs is tracked using species HCHO_X1. Both species undergo the same photolysis reactions:

$$HCHO + h\nu \rightarrow 2HO_2 + CO \qquad \text{(R2.2)}$$

$$HCHO\_X1 + h\nu \rightarrow 2HO_2 + CO \qquad \text{(R2.2')}$$

By applying reaction rate analysis on the two reactions, the contributions freshly emitted and secondary HCHO to the generation of HO_2, and subsequently to OH can be directly determined.

Figure 2.5(a) shows the regional distribution of episode-average P_{OH} and major sources and sinks of OH predicted by the S07C mechanism between 12:00-13:00 CST at the surface layer, and the difference between the S07C and S99 predictions. P_{OH} is highest in the urban and industrial regions with values approximately 0.85-0.9. The S99 predictions are similar to S07C in urban, industrial areas and over the ocean while in rural areas S99 predictions are lower by approximately -0.06-0.08. Reactions of OH with VOCs and CO account for majority of the reacted OH in most part of the domain although in urban areas OH reactions with inorganic compounds are also important (Figure 2.5(b) and Figure 2.5(c)). The key inorganic reaction is the OH + NO_2 termination reaction. The S07C predictions are lower, mainly because OH concentrations in the S07C are lower than those in S99. Figure 2.5(d) shows the amount of total regenerated OH (excluding HO_2 from the photolysis of freshly emitted VOCs) is approximately 10-15 ppb and the S07C predictions are approximately 10-15% lower than the S99 results. Figure 2.5(e) shows that the amount of new OH generated in this hour ranges from 1.6-3.2 ppt and S07C predictions are lower than S99 predictions by as much as 0.85 ppt (approximately 25%). The higher new OH formation rate in S99 explains the differences in the predicted OH concentrations, as shown in Figure 2.5(f).

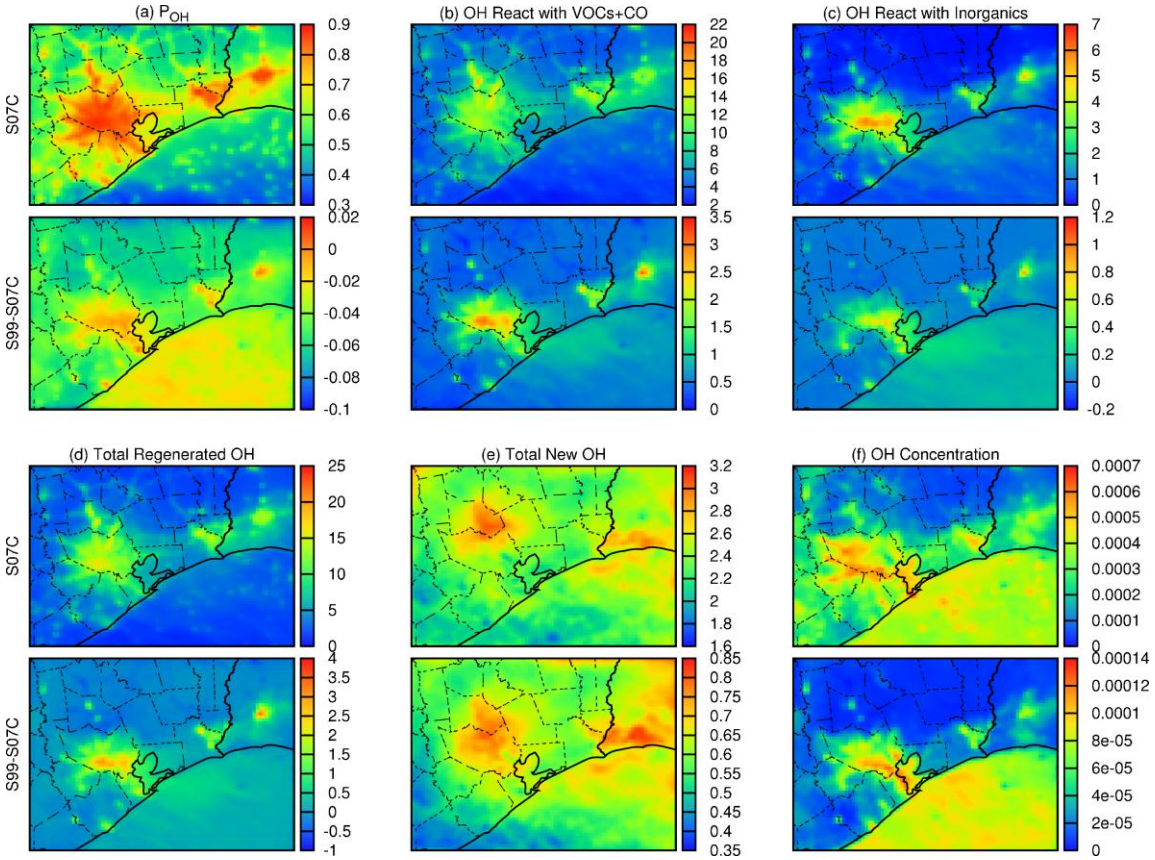

Figure 2.5 (a) Regional distributions of the O_3 propagation factor (P_{OH}), (b) the rate of OH reacted with VOCs and CO, (c) the rate of OH reacted with other inorganic species, (d) the overall rate of OH regeneration, (e) the rate of OH regeneration due to HO2 from photolysis of VOCs and (f) the rate of new OH formation from $H_2O + O(^1D)$ reaction. Results are based on episode averaged for hour 12:00-13:00 CST. Units for panel (b)-(f) are ppm hr^{-1}. The scales of the panels are different to show the details of the spatial distribution.

Oxides of nitrogen (NOx) are also important precursors of O_3 in the troposphere. It is convenient to define the propagation factor P_{NO}, similar to its counterpart P_{OH}, as a measure to quantify the efficiency of NO in the photochemical mechanisms. NO could react with both inorganic species and organic species to form NO_2, which could regenerate NO through photolysis reaction. However, not all reacted NO molecules can be regenerated as some react with organics to form more stable organonitrate. The P_{NO} in

this modeling episode is very close to unity and the predictions of the S07C are slightly higher than the S99 predictions in the urban areas (Figure 2.6(a)). At 12:00-13:00 CST, most of the NO is consumed by reacting with organic radicals with a rate of 0.4-0.8 ppm hr^{-1} in the Houston area (Figure 2.6(b-c)). This is mostly balanced by the rapid photolysis of NO_2 (Figure 2.6(d-f)). The S07C predictions of the NO consumption by organic radicals are approximately 5-10% higher than the S99C results.

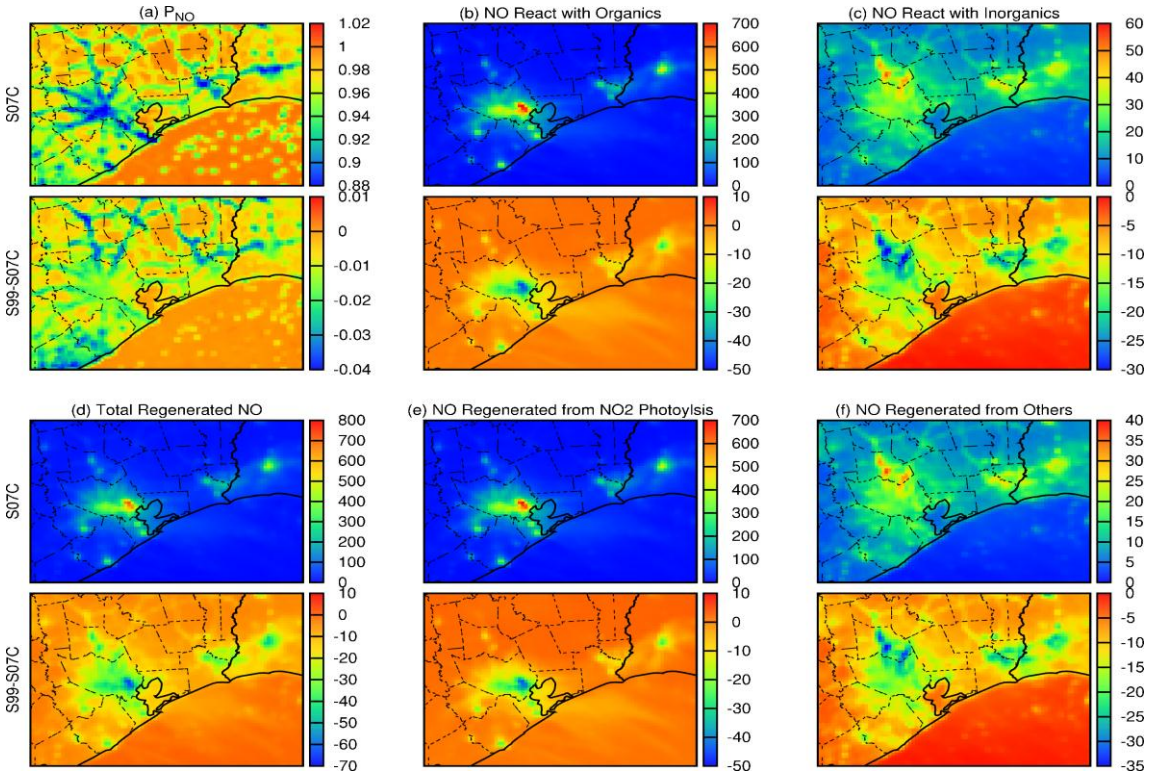

Figure 2.6 (a) Regional distributions of the O_3 propagation factor (P_{NO}), (b) the rate of NO reacted with organics, (c) the rate of NO reacted with other inorganic species, (d) the overall rate of NO regeneration, (e) NO regeneration due to NO_2 from photolysis and (f) NO regeneration formation from reactions other than NO_2 photolysis. Results are based on episode averaged for hour 12:00-13:00 CST. Units for panel (b)-(f) are ppm hr^{-1}. The scales of the panels are different to show the details of the spatial distribution.

Figure 2.7 shows the time series of episode-average OH budget at C35C and CONR predicted by S99 and S07C. P_{OH} at C35C ranges from 0.85-0.9 during the day and S07C predictions are very similar to S99. Although more OH reacts with VOCs and inorganics in S99 (Figure 2.7(c)), more OH is regenerated (Figure 2.7(d)). This indicates that an OH in S99 and S07C mechanisms is able to oxidize similar amount of VOC molecules before being removed from the system. However, the predicted OH concentrations by S99 and S07C are significantly different. S99 predicts much higher OH concentrations (peak OH is approximately 0.5ppt at 12:00-13:00 CST) than S07C (peak OH is approximately 0.4 ppt) throughout the day, which is caused by the faster new OH formation from $H_2O + O(^1D)$ reaction in S99. This is mainly because the reaction rate constant of this reaction is reduced by approximately 10% from 2.2×10^{-10} $cm^3molecule^{-1}s^{-1}$ in S99 to 1.99×10^{-10} $cm^3molecule^{-1}s^{-1}$ in S07C. The amount of new OH formation from photolysis of freshly emitted VOCs is approximately the same. At CONR, the P_{OH} values are lower than those at C35C and the difference between S99 and S07C results are more significant. Minimal P_{OH} is 0.6 and 0.7, predicted by S99 and S07C, respectively (Figure 2.7(b)). Although S99 predicts more new OH production, it predicts similar OH concentrations as S07C, because of the lower P_{OH} values. The lower P_{OH} at CONR is mostly caused by the difference in the regenerated OH from photolysis of secondary VOCs, in which S07C predictions are higher (Figure 2.7(d)).

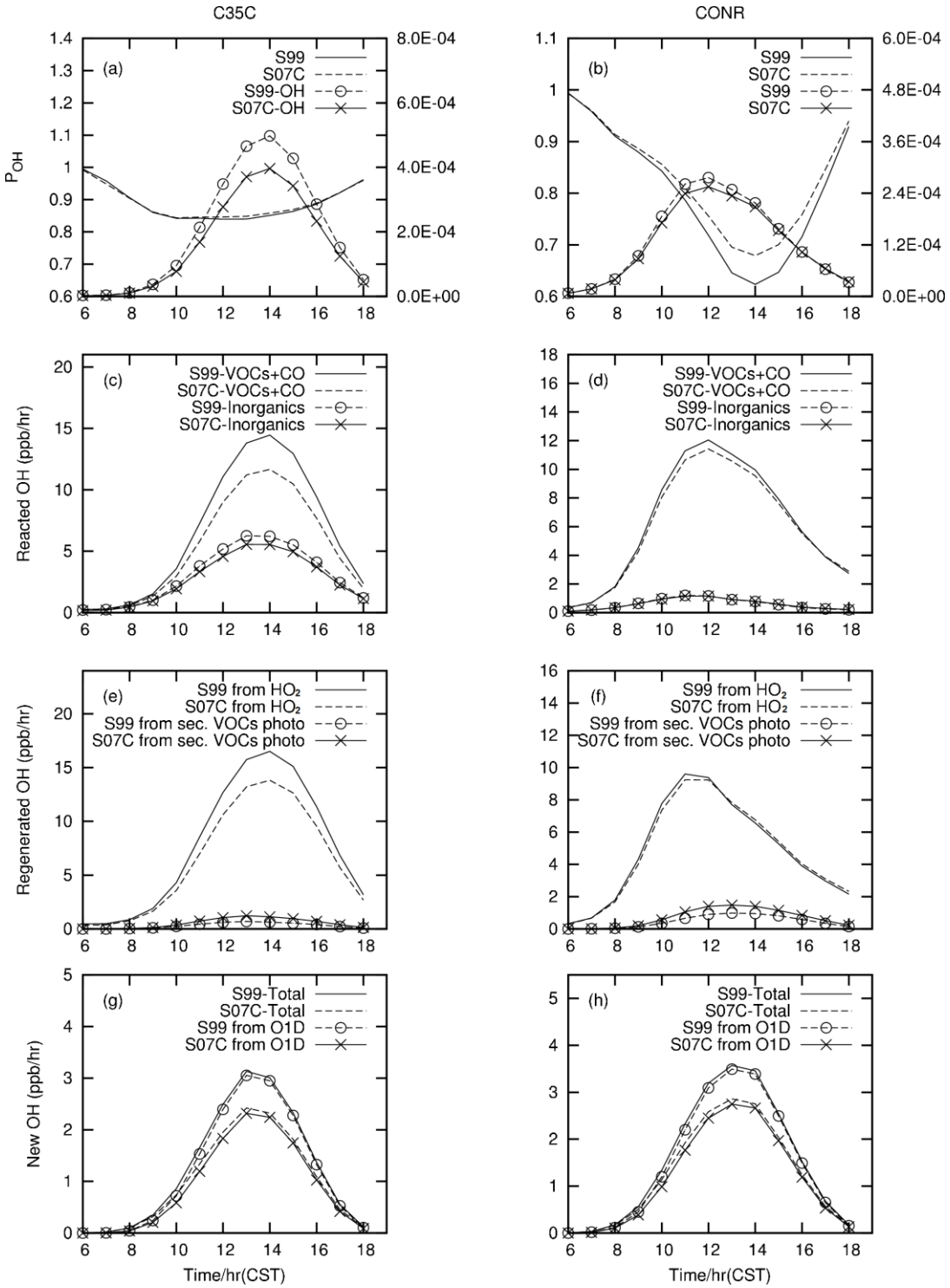

Figure 2.7 Time series of episode-average of P_{OH}, reacted OH, regenerated OH and new OH at C35C and CONR. OH concentration is also shown along with P_{OH} (on panel (a) and (b)). The units for OH concentration are ppb.

Figure 2.8 shows the vertical distribution of P_{OH} and sources and sinks of OH at C35C and CONR at 12:00-13:00 CST. At C35C, P_{OH} decreases from 0.75-0.85 near the surface to 0.3-0.4 at 3000 meters above surface (Figure 2.8(a)). S99 predictions are slightly lower than S07C, and the differences between the two mechanisms increase as a function of height above surface. Reacted OH with VOCs+CO and with inorganics also decrease as height increases (Figure 2.8(c)). The highest value of reacted OH with inorganics is about 6.2 ppb at surface layer predicted by S99, the differences between S99 and S07C is about 1 ppb at this level. Reacted OH with VOCs+CO is approximately 2 times higher than that with inorganics. Differences decrease as height increase, and two mechanisms predict similar reacted OH with inorganics above 1000m. The amount of regenerated OH from HO_2 decreases as a function of height, with S99 predictions slightly higher than S07C (Figure 2.8(e)). At elevations above 2000 m, most of the regenerated OH is from photolysis of secondary VOC but near the surface secondary VOC only accounts for a small fraction of the total regenerated OH. New OH from $H_2O+O(^1D)$ reaction accounts for almost all "new" OH production in all the layers. New OH production increases as height up to 1000 m (Figure 2.8(g)). S99 predicts a peak new OH production of 3.8 ppb while S07C prediction is approximately 1 ppb lower. The difference between S07C and S99 decreases above 1000 m. The vertical profiles at CONR is similar although the differences in the reacted and regenerated OH between S07C and S99 are less than those at C35C. The difference in the new OH between the two mechanisms at CONR is similar to those at C35C, with S99 predictions approximately 0.7-1 ppb higher than those of S07C.

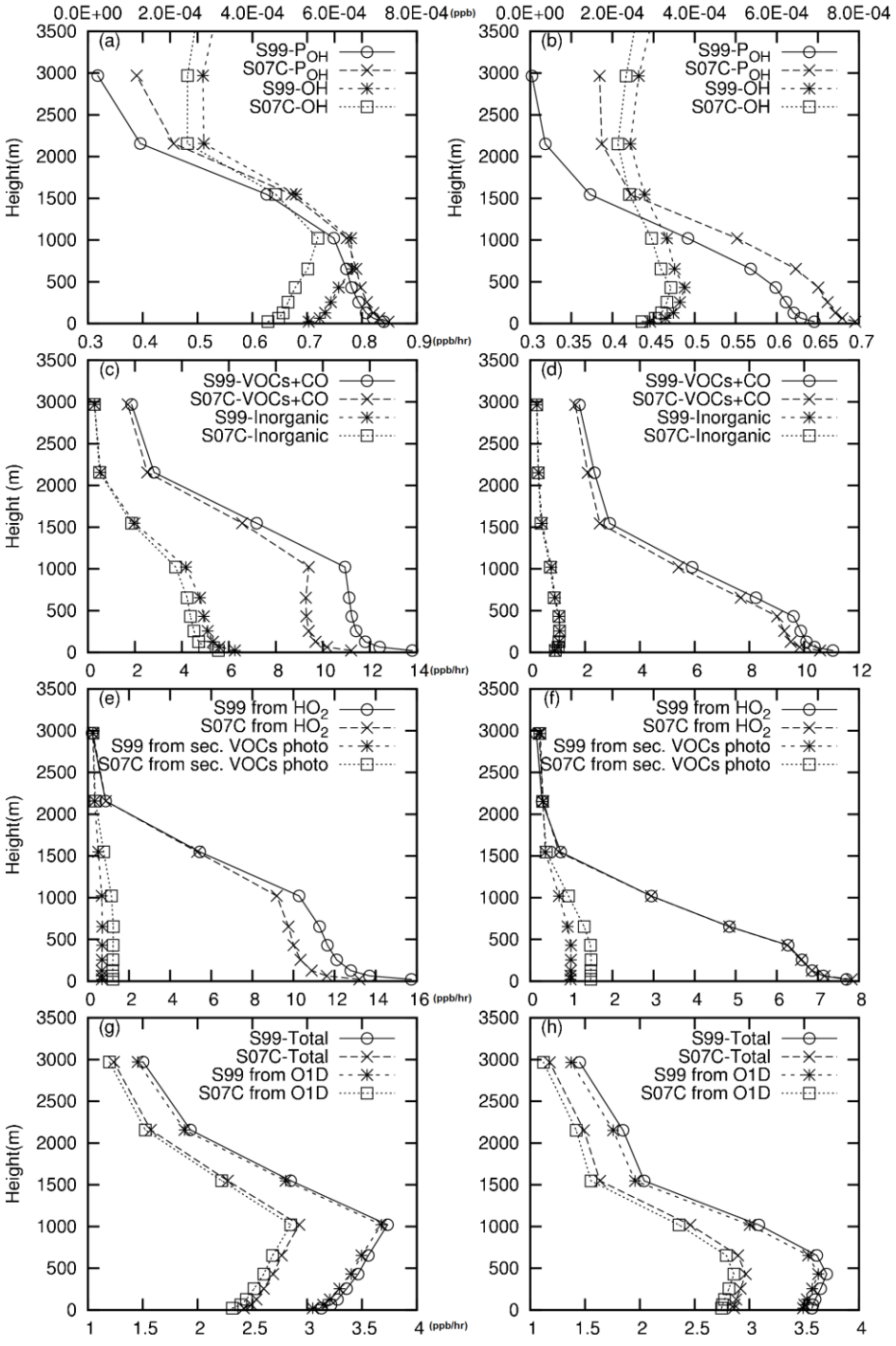

Figure 2.8 Episode-average of P_{OH}, reacted OH, regenerated OH and new OH at different height level. Left column is results at C35C, the right column is that at CONR. OH concentrations are also shown in (a) and (b), and units are ppb along with P_{OH}. Units in (c)-(h) are ppb/hr.

Figure 2.9 shows that there is no significant different between S07C and S99 in the NO cycle. The NO propagation factor approximately 0.9 at C35C and close to 1.0 at CONR. This suggests that most of the reacted NO is regenerated and less the 10% is lost to form stable products. NO reactions are much faster at C35C than CONR.

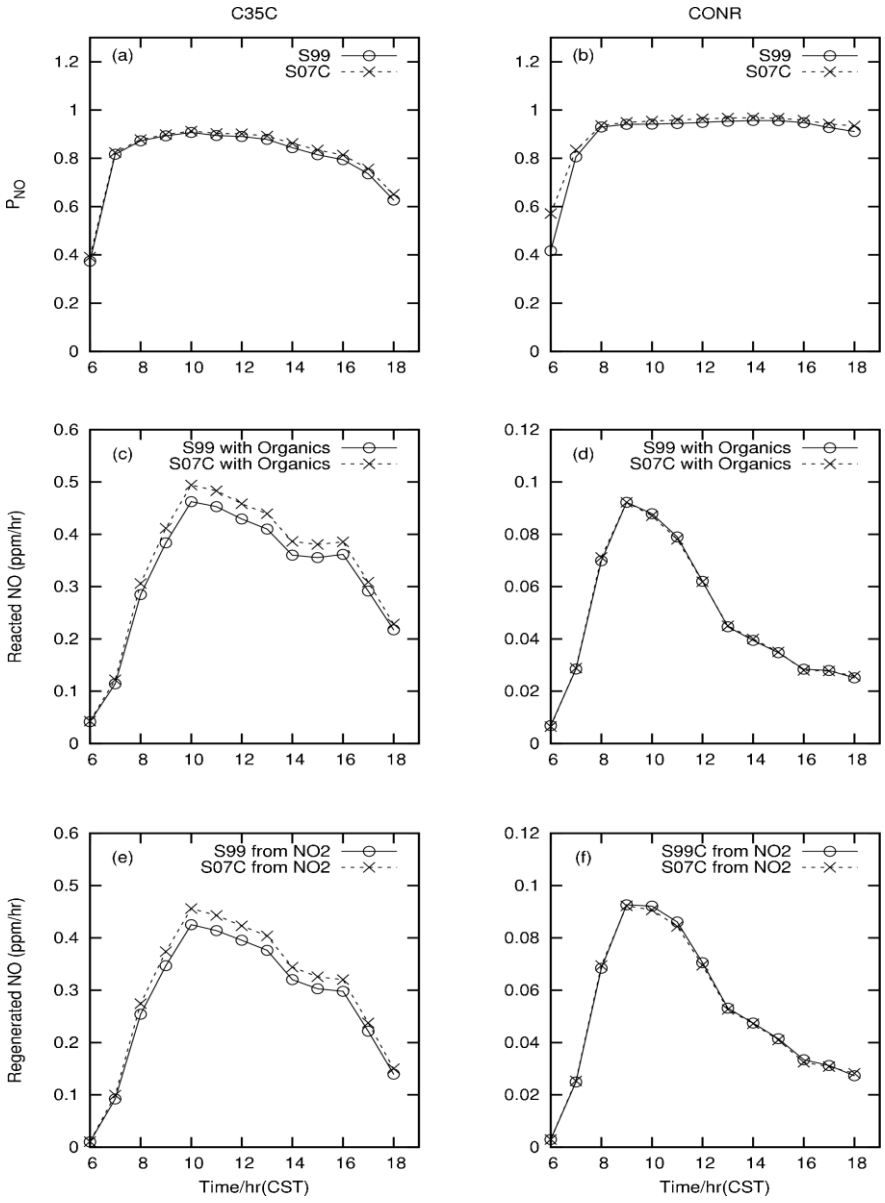

Figure 2.9 Time series of episode-average (a) PNO, (b) reacted NO and (c) regenerated NO at C35C.

2.3.3 Response to emission reductions

One of the regulatory applications of the photochemical modeling is to demonstrate the effectiveness of proposed emission reduction in improving air quality. The US EPA recommends that the relative response factor (RRF) and O_3 design values (DV) should be used instead of the predicted concentrations for O_3 attainment demonstrations. The RRF is defined as the ratio of the predicted average 8-hr maximum O_3 concentrations near a monitoring station on high O_3 days under a hypothetical future year emission scenario to the predicted average 8-hr maximum O_3 concentrations on the same days using the base year emission inventory. The days used for average 8-hr O_3 calculations are chosen based on the base year 8-hr O_3 concentrations. Once the RRF is determined, the O_3 design value (DV) for the future year under the hypothetical future year emission scenario can be calculated by multiplying the RRF with the baseline design value, which is the average of the fourth highest monitored daily 8-hour maximum value at each monitoring site during a 5 year period that saddles the base case inventory year. More details of the calculation of the RRF and DV can be found in the EPA document.

In this study, 25 simulations are conducted by systematically scaling the anthropogenic emissions of NOx and VOC by a factor of 0.6, 0.8 1.0, 1.2 and 1.4 throughout the entire 4km domain for both S99 and S07C mechanisms. The days with 8-hr maximum O_3 greater or equal 70 ppb under base case emission scenarios (both NOx and VOC scaling factors are 1.0) are considered as high O_3 days for the RRF calculation. The 4 km resolution grid cells within a 7x7 grid array centered on a monitoring station

are considered near the monitoring station and the averaged O_3 concentrations of these grid cells are used in the RRF calculation.

Figure 2.10 shows the isopleths of the RRF for 8-hr maximum O_3 concentration at the five stations based on S99 (first column) and S07C (second column) and the ratio of RRF S99 and RRF S07C (third column). At CONR, both S99 and S07C predict that RRF is not sensitive to VOC changes but is more response to NOx changes. Both predict that 60% reduction in domain-wide anthropogenic NOx emissions will lead to approximately 7% reduction in the predicted 8-hr O_3 concentrations. S99 always predicts slightly lower RRF values than S07C at this location and the minimum ratio is 0.997. At HALC, both mechanisms predict that the RRF is more responsive to NOx changes rather than VOC changes. A combined reduction of VOC and NOx by 60% leads to a reduction of ozone by approximately 6-7%. At HCFA and C35C, both mechanisms predict that the RRF value is more responsive to VOC changes under higher NOx emissions (scaling factors of NOx greater than 1.0) while is more responsive to NOx changes under lower NOx emissions (scaling factors of NOx lower than 1.0). At DRPK, both mechanisms predict that the RRF values are more responsive to VOC changes. Reducing NOx emissions does not significantly change the RRF but increasing NOx leads to decrease in RRF. Thus, the DRPK site is under NOx saturated condition based on the base case emission inventory. The maximum difference in the RRF between the two mechanisms is generally highest under lowest VOC+highest NOx or highest VOC+lowest NOx. Under all emission scaling scenarios, the difference in the RRF values predicted by the two mechanisms is less than 1%.

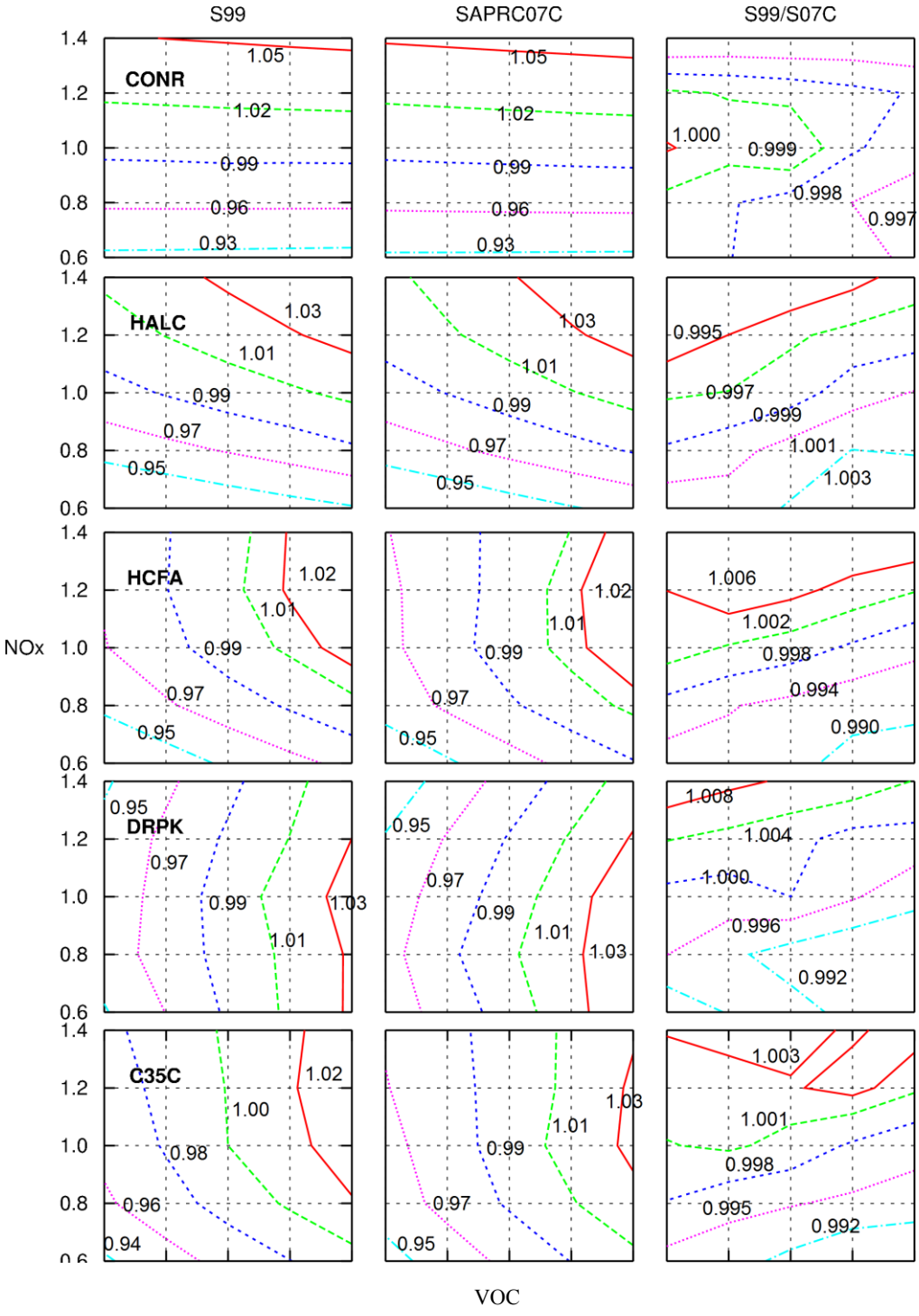

Figure 2.10 Isopleths of maximum 8-hr O_3 average as a function of relative VOC and NO_x emission ratios predicted by CMAQ model with S99 and S07C mechanisms. Last column shows the difference in the isopleths.

2.4 Conclusions

The SAPRC07 (S07) photochemical mechanism, an update from SARPC99 (S99) - the last SAPRC photochemical mechanism, is implemented into the Community Multi-scale Air Quality (CMAQ) model and applied to simulate a high ozone episode during the 2000 Texas Air Quality Study (TexAQS 2000). The results from the S07 mechanism are compared with those from the SAPRC99 model, which is last version of the SAPRC mechanism. In general, the predicted ozone concentrations by S07C are lower than those of S99 with maximum difference as high as 20%. The two mechanisms also show significant difference in the predicted OH, PAN, HCHO and HNO_3 concentrations. The difference in the OH concentrations (S99 is higher by 8-20%) is partly due to the difference in the OH + NO_2 reaction rate coefficients. The difference of HNO_3 is most significant at night, and is due to the additional of an additional NO_2 homogeneous reaction with H_2O. The difference in PAN (S99 higher by approximately 15%) is due to the PAN photolysis reactions included in S07 but not in S99. The difference in HCHO (S99 higher by approximately 15%) is also due to the difference in the photolysis rate of HCHO in the two models. Although the two mechanisms predict different ozone concentrations, the relative response factor (RRF) of ozone at rural, urban and industrial sites under emission controls of anthropogenic NOx and VOC controls by factors 0.6 – 1.4 predicted by the two mechanisms are very similar. This suggests that although the absolute predictions are different, both models will give nearly identical attainment assessment in regulatory applications.

3. IMPLEMENTATION AND INITIAL APPLICATION OF THE NEAR-EXPLICIT MASTER CHEMICAL MECHANISM IN THE 3D COMMUNITY MULTI-SCALE AIR QUALITY (CMAQ) MODEL

3.1 Model Description

CMAQ v4.6 was used as the host model to implement the most recent version of the MCM model (MCM v3.1, downloaded from http://mcm.leeds.ac.uk/MCM/). The inorganic chemistry part of the original MCM v3.1 was replaced with reactions from an expanded version of the standard SAPRC07 photochemical mechanism (Carter, 2010 (quotation is wrong)), the most recent update of the widely used SAPRC99 photochemical mechanism (Carter, 2000). No changes were made to the organic chemistry part of the MCM v3.1 mechanism. The final gas phase photochemical mechanism contains 4642 species and 13566 reactions.

The photolysis rates are based on the most recent updates of the quantum yield and absorption cross section data (Table 3.1) and are calculated using the JPROC tool in CMAQ rather than using the original MCM fitted functions (Jenkin et al., 1997) so that clear sky photolysis rates can be better estimated as a function of height. The dry deposition velocity of most of the species in the original MCM model is a constant value. In the CMAQ-MCM, the dry deposition rates of the VOC species are calculated based on 8 existing CMAQ dry deposition surrogates. Horizontal and vertical transport processes are considered only for non-radical species. The SMVGEAR solver (Jacobson and Turco, 1994) included in the CMAQ distribution is used to solve the ordinary

differential equations that describe the change of species concentrations in the gas phase due to photochemical reactions as a function of time. The SMVGEAR solver has been applied in previous studies and demonstrated to be efficient for the MCM mechanism (Liang and Jacobson, 2000).

Table 3.1 Photolysis reactions for organic compounds in MCM and the source of data for spectral quantum yield and absorption cross section data

Reaction		Source of Data
Carbonyls		
HCHO	→ HCO + H	IUPAC 2002, Photolysis of organic species, P1
	→ CO + H_2	
CH_3CHO	→ HCO + CH_3	IUPAC 2002, Photolysis of organic species, P2
C_2H_5CHO	→ HCO + C_2H_5	IUPAC 2002, Photolysis of organic species, P3
n-C_3H_7CHO	→ HCO + n-$C_3H_7^*$	IUPAC 2002, Photolysis of organic species, P11
	→ CH_3CHO + C_2H_4	
i-C3H7CHO	→ HCO + i-$C_3H_7^*$	Martinez et al. (Martinez et al., 1992)**
CH_2=C(CH_3)CHO	→ CH_3C=CH_2 + HCO*	IUPAC 2002, Photolysis of organic species, P9
	→ CH_2=C(CH_3)CO + H*	
$CH_3C(O)CH_3$	→ CH_3CO + CH_3	IUPAC 2005, Photolysis of organic species, P7
$CH_3C(O)C_2H_5$	→ CH_3CO + $C_2H_5^*$	IUPAC 2005, Photolysis of organic species, P8
$CH_3C(O)CH$=CH_2	→ CH_3CH=CH_2 + CO	IUPAC 2002, Photolysis of organic species, P10
	→ CH_3CO + CH=CH_2^*	
A-Dicarbonyls		
$(CHO)_2$	→ 2CO + H_2	IUPAC 2005, Photolysis of organic species, P4
	→ CO + HCHO	
	→ HCO + HCO	
$CH_3C(O)CHO$	→ CH_3CO + HCO*	IUPAC 2003, Photolysis of organic species, P6
$CH_3C(O)C(O)CH_3$	→ CH_3CO + CH_3CO^*	Plum et al. (Plum et al., 1983)**
Hydroperoxides		
CH_3OOH	→ CH_3O + OH*	IUPAC 2002, Photolysis of organic species, P12
Organic Nitrates		
CH_3ONO_2	→ CH_3O + NO_2	IUPAC 2002, Photolysis of organic species, P14
$C_2H_5ONO_2$	→ C_2H_5O + NO_2	IUPAC 2002, Photolysis of organic species, P15
n-$C_3H_7ONO_2$	→ n-C_3H_7O + NO_2^*	IUPAC 2002, Photolysis of organic species, P16
i-$C_3H_7ONO_2$	→ i-C_3H_7O + NO_2^*	IUPAC 2002, Photolysis of organic species, P17
t-$C_4H_9ONO_2$	→ $CH_3C(O)CH_2O$ + NO_2^*	IUPAC 2002, Photolysis of organic species, P18
$CH_3C(O)CH_2ONO_2$	→ CH_3CO + HCHO + NO_2^*	Barnes et al. (Barnes et al., 1993)**

*These reactions are also used to define the photolysis rates of a large number of related species.
** Not available from IUPAC so they are based on the original source of data cited in Jenkin et al. (1997).

3.2 Model Application

The CMAQ-MCM model is applied to a three-week high ozone episode (August 16 to September 6, 2000) during the 2000 Texas Air Quality Study (TexAQS 2000) using a three-level nested domain (Figure 3.1). The coarse domain is for the eastern United States with 36 km horizontal resolution. The 12 km inner domain covers the eastern Texas and surrounding states. The Houston-Galveston Bay (HGB) and Beaumont-Port Arthur (BPA) areas in southeast Texas are modeled with a 4 km horizontal resolution domain (referred to as the 4 km domain hereafter). For all the three domains, the vertical extent of the CMAQ model is divided into 14 layers. The first layer thickness is approximately 33 m. More details of the model setup can be found in Ying and Krishnan (2010). Meteorology inputs needed to drive the CMAQ-MCM model are generated from MM5 mesoscale meteorology simulation results from the Texas Commission of Environmental Quality (TCEQ). The boundary and initial conditions (BCs and ICs) of inorganic species (O_3, NO, NO_2, NO_3, N_2O_5, HNO_3, HNO_4, H_2O_2, CO and SO_2) for the 36 km parent domain are based on the default CMAQ profiles. For organics, only HCHO (formaldehyde), PAN (peroxyacetyl nitrate), MVK (methyl vinyl ketone), C_2H_2 (ethylene) and C_5H_8 (isoprene) are included in the BCs and ICs of the 36 km domain simulation, as they are directly available from the default CMAQ profiles. BCs and ICs for other organic species are set to zero. This practice is not expected to affect the model results significantly, especially for the nested domains, since emissions from sources within the parent domains are expected to be much more significant than the contributions from BCs. The first two days are considered as spin-up days and the results for those days are

not included in the final analysis.

EPA's 2001 CAIR (Clean Air Interstate Rules) emission inventory is used to generate emission inputs for the TexAQS 2000 episode. Pre-calculated monthly on-road vehicle emissions in the 2001 EPA CAIR inventory are directly used to calculate hourly on-road mobile source emissions. Emissions of inorganic species and detailed VOC species are processed using a modified Sparse Matrix Operator Kernel Emissions (SMOKE) program from US EPA. VOC speciation profiles are taken from a comprehensive speciation database SPECAITE 3.2 (http://www.epa.gov/ttnchie1/software/speciate/speciate32.html). Biogenic emissions are processed using Biogenic Emission Inventory System (BEIS) v3.14 within SMOKE (Vukovich and Pierce, 2002). Monoterpenes that are not represented by the MCM species are mapped to α-pinene if they have endocyclic double bonds or β-pinene if they have exocyclic double bonds (Johnson et al., 2006b). The emissions of anthropogenic VOCs that are not represented by the MCM species are ignored in the emission processing. This ensures a more accurate comparison of the model predictions with observations of detailed VOCs. Approximately 95% of reactive VOC emissions in the 4 km domain have been represented by 135 MCM VOC species. Table 3.2 lists the emission rates of major VOC species represented by the MCM model in the 4 km domain on a typical week day from 7 different emission source categories.

Table 3.2 Emission rates of major VOC species in the 4km domain on August 31, 2000*

	S1	S2	S3	S4	S5	S6	S7
ethane	0.000	3.015	2.028	13.595	0.149	20.185	16.373
propane	0.000	0.261	0.789	18.762	0.198	7.122	0.000
n-butane	0.000	38.848	14.699	14.131	0.261	5.756	0.000
isobutane	0.000	1.443	2.600	2.943	0.469	1.729	0.000
n-pentane	0.247	10.237	4.349	12.059	0.275	3.476	0.000
isopentane	0.247	19.253	9.875	7.522	0.093	1.589	0.000
3-methylpentane	0.225	4.284	1.628	1.784	0.074	0.236	0.000
n-hexane	0.000	3.437	1.317	6.424	0.581	4.012	0.000
2,2-dimethylbutane	0.000	1.753	0.309	1.482	0.072	0.121	0.000
cyclohexane	0.000	0.138	1.972	0.802	0.412	0.907	0.000
2,3-dimethylbutane	0.450	3.283	1.031	2.064	0.075	0.239	0.000
2-methylpentane	0.225	2.518	2.648	1.671	0.074	0.236	0.000
n-heptane	0.000	0.884	0.959	4.368	2.313	3.757	0.000
3-methylhexane	0.151	1.559	1.493	1.000	0.066	0.098	0.000
2-methylhexane	0.151	1.557	0.000	0.983	0.087	0.093	0.000
n-octane	0.000	0.458	0.451	1.870	0.074	2.597	0.000
n-nonane	0.000	0.114	0.274	0.272	0.311	0.130	0.000
n-decane	0.000	0.288	0.260	0.615	0.312	0.565	0.000
n-undecane	0.000	0.586	0.755	0.407	0.567	0.211	0.000
ethylene	4.176	7.684	5.784	16.361	0.026	7.909	67.662
propylene	1.090	3.206	1.588	5.011	0.080	3.911	67.670
trans-2-butene	0.000	0.529	0.828	0.393	0.000	0.444	0.000
cis-2-butene	0.000	0.351	0.745	0.046	0.000	0.044	0.000
1-butene	0.854	0.776	1.264	0.974	0.031	1.709	30.018
1-pentene	0.000	0.881	0.475	0.382	0.079	2.857	0.000
trans-2-petene	0.000	1.852	1.007	0.233	0.001	0.467	0.000
cis-2-pentene	0.000	1.044	0.593	0.194	0.001	0.462	0.000
acetylene	0.000	4.216	1.216	1.577	0.007	1.816	0.000
benzene	0.000	8.011	2.063	8.111	0.806	3.848	0.000
toluene	0.000	19.540	7.420	6.253	17.68	3.148	0.000
o-xylene	0.000	3.052	2.252	2.101	2.791	1.126	0.000
m-xylene	0.000	7.957	0.112	2.423	0.858	1.621	0.000
p-xylene	0.000	0.066	3.606	3.055	0.838	0.938	0.000
ethylbenzene	0.000	3.011	1.125	1.795	1.104	1.096	0.000
styrene	0.000	0.498	0.000	3.419	0.197	1.022	0.000
1,3,5trimethylbenze	0.000	1.191	2.707	0.415	0.207	0.179	0.000
1,2,4trimethylbenze	0.000	3.267	3.326	0.426	0.229	0.172	0.000
1,2,3trimethylbenze	0.000	0.649	0.945	0.418	0.216	0.124	0.000
n-propylbenzene	0.000	0.807	0.695	0.367	0.056	0.077	0.000
iso-propylbenzene	0.000	3.011	1.125	1.795	1.104	1.096	0.000
o-ethyltoluene	0.000	1.056	0.296	0.345	0.041	0.090	0.000
m-ethyltoluene	0.000	3.114	1.503	0.345	0.040	0.116	0.000
p-ethyltoluene	0.000	0.293	0.000	0.344	0.042	0.078	0.000
formaldehyde	1.802	1.610	1.043	5.884	0.157	8.123	64.263
acetaldehyde	0.609	0.790	0.395	0.870	0.042	0.781	47.133
acetone	0.000	0.688	0.000	1.509	0.920	1.334	93.401

Table 3.2 continued

	S1	S2	S3	S4	S5	S6	S7
isoprene	0.000	0.245	0.105	0.036	0.056	0.331	2046.80
α-pinene	0.000	0.000	0.000	4.275	0.003	0.378	470.333
β-pinene	0.000	0.000	0.000	2.793	0.002	0.245	206.878
Total	**10.226**	**173.313**	**89.659**	**164.90**	**34.075**	**98.601**	**2937.71**

***Units are SI tons day^{-1}

S1: Diesel Vehicle; S2: Highway Gasoline; S3: Off Highway Gasoline; S4: Industry; S5: Solvent; S6: Other; S7: Biogenic

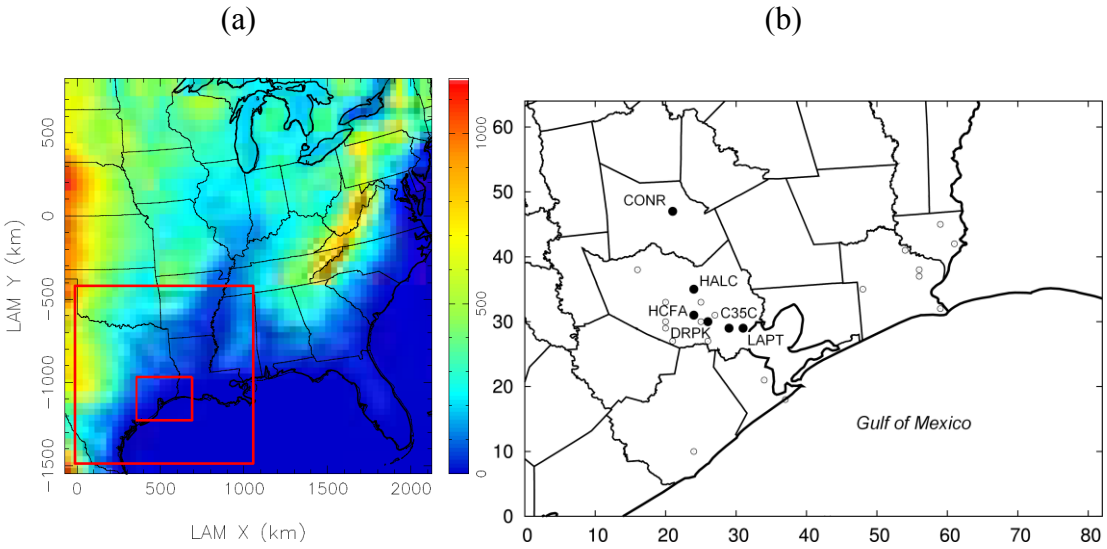

Figure 3.1 (a) Modeling domains used in the study. Boxes show the East Texas and Southeast Texas nested domains. Colors represent surface elevation above sea level. (b) Locations of major monitoring stations in the 4 km resolution Southeast Texas domain.

3.3 Results and Discussions

3.3.1 Comparison with observations and lumped mechanism SAPRC07

The predicted gas phase species concentrations from the CMAQ-MCM are compared with observations and also results from a separate CMAQ simulation that uses the expanded standard SAPRC07 (Carter, 2010) as the gas phase photochemical

mechanism (CMAQ-SAPRC07). Identical meteorology and raw emission database are used in the CMAQ-SAPRC07 simulation. VOC speciation profiles for the SAPRC07 are also based on SPECIATE 3.2 and generated using a program developed by W.P.L. Carter (http://www.cert.ucr.edu/~carter/emitdb/).

Figure 3.2 shows that the predicted O_3 concentrations from the CMAQ-MCM model generally agree well with the observations. The under-prediction of the peak O_3 concentrations on some days has been attributed to the underestimation of highly reactive volatile organic compounds (HRVOCs) emissions from industrial sources and O_3 performance can be improved by increasing the alkene emissions from industrial sources by a factor of 5 (Ying and Krishnan, 2010). In order to evaluate the raw emission inventory to quantify the bias in the alkene predictions, no alkene emission adjustments were used in this study. Generally the MCM predicted O_3 concentrations are very similar to but slightly higher than those of CMAQ-SAPRC07, which can be seen in Figure 3.2 and from the O_3 model performance statistics (Table 3.3). Time series of NO_2 and CO in Figure 3.3-3.4 show that the MCM predictions are also very similar to the SAPRC07 results and are in good agreement with observations.

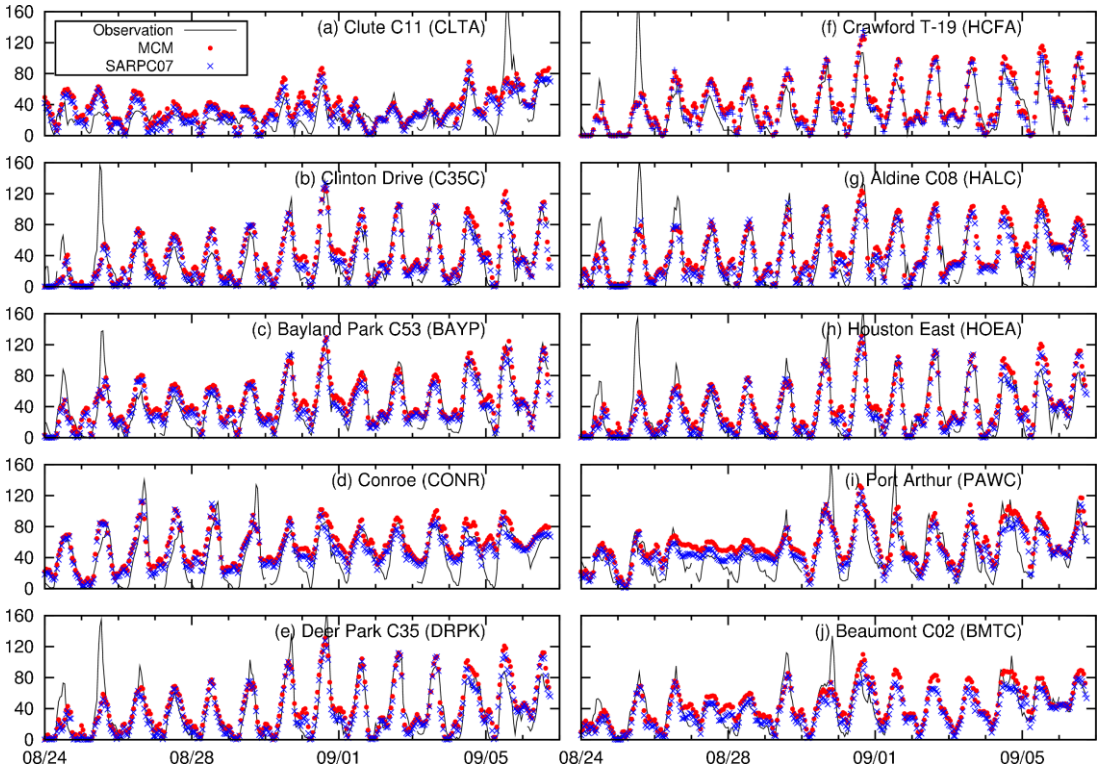

Figure 3.2 Predicted and observed O_3 concentrations in HGB and BPA areas. Units are ppb.

Table 3.3 Statistical model performance analysis for ozone

	MCM		SAPRC07			MCM		SAPRC07		
	MFB	**MFE**	**MFB**	**MFE**	**NP**	**AUP**	**AAUP**	**AUP**	**AAUP**	**NP**
BAYP	-0.06	0.32	-0.16	0.29	24	-0.09	0.39	-0.17	0.34	4
C35C	0.15	0.21	0.02	0.11	71	0.09	0.24	0.01	0.16	15
CLTA	-0.02	0.14	-0.13	0.17	74	-0.15	0.22	-0.20	0.23	16
CONR	-0.05	0.23	-0.13	0.24	71	-0.17	0.28	-0.21	0.28	18
DRPK	0.07	0.19	-0.04	0.17	98	0.02	0.15	-0.03	0.10	18
HALC	0.06	0.20	-0.02	0.17	78	-0.08	0.23	-0.11	0.21	19
HCFA	0.04	0.16	-0.02	0.16	65	-0.04	0.18	-0.09	0.18	15
HOEA	0.06	0.17	-0.05	0.17	67	-0.07	0.27	-0.12	0.25	15
PAWC	0.05	0.19	-0.07	0.20	75	-0.05	0.21	-0.13	0.20	17
BMTC	0.09	0.22	0.00	0.18	52	-0.08	0.25	-0.13	0.25	9

MFB: mean fractional bias, MFE: mean fractional error, AUP: accurancy of unpaired peak, AAUP: absolute accurancy of unpair peak, NP: number of data points. For MFB and MFE analysis, a threshold observed 1-h averaged ozone concentration of 60 ppb is applied. For AUP and AAUP analysis, a threadhold observed peak ozone of 60 ppb is also applied. See below for definition of these statistical measures.

$$MFB = \frac{2}{N}\sum_{i=1}^{N}\frac{P_i - O_i}{P_i + O_i}; MFE = \frac{2}{N}\sum_{i=1}^{N}\frac{|P_i - O_i|}{P_i + O_i}; AUP = \frac{1}{N}\sum_{i=1}^{N_d}\frac{P_{p\_peak,i} - O_{o\_peak,i}}{O_{o\_peak,i}}; AAUP = \frac{1}{N_d}\sum_{i=1}^{N_d}\left|\frac{P_{p\_peak,i} - O_{o\_peak,i}}{O_{o\_peak,i}}\right|$$

N is the number of 1-hr concentration data points, N_d is number of days, P_i is the prediction and O_i is the observation at hour i, $P_{p\_peak,i}$ is the predicted ozone peak at the i^{th} day and $O_{o\_peak,i}$ is the observed ozone peak at the i^{th} day.

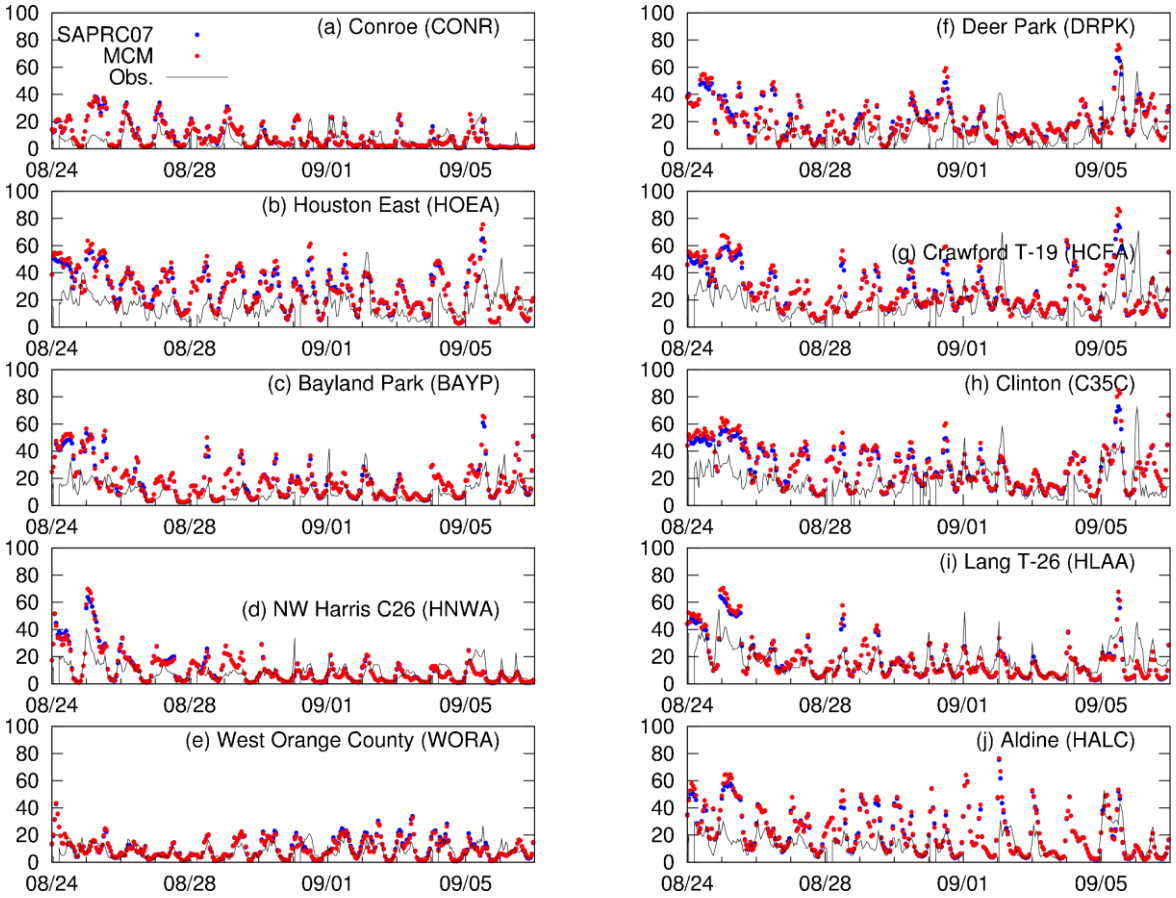

Figure 3.3 Predicted and observed NO_2 concentrations in HGB and BPA areas. Units are ppb.

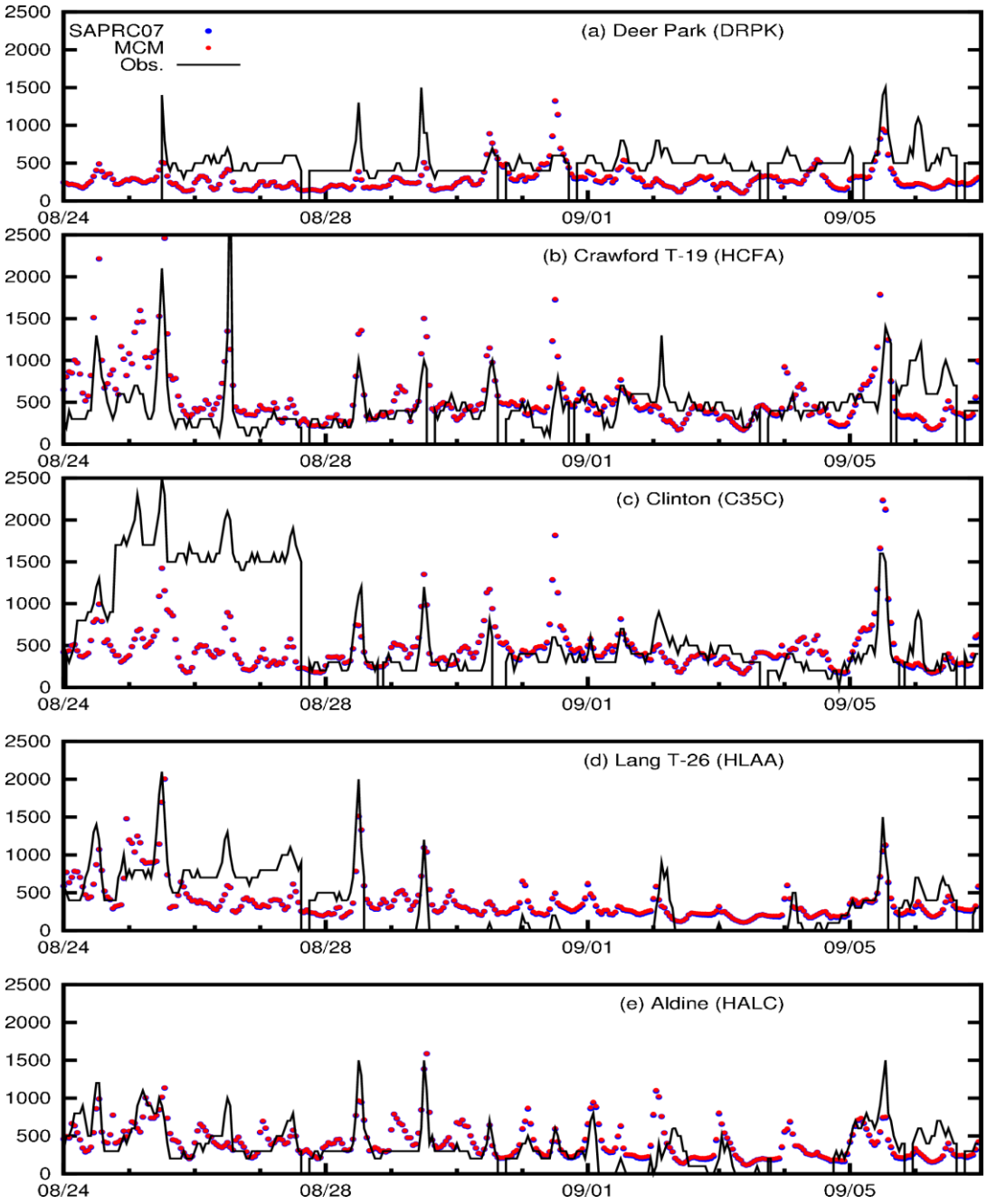

Figure 3.4 Predicted and observed CO concentrations in HGV and BPA areas. Units are ppb.

Figure 3.5 compares episode-average hourly concentrations of several species that are explicitly modeled by both the MCM and the SAPRC07 mechanisms at 5 monitor

sites. The 5 sites represent suburban (CONC), urban (HALC, HCFA, DRPK) and industrial (C35C) locations in the HGB area. O_3 concentrations from the MCM mechanism are slightly higher than the SAPRC07 predictions at all five locations at all hours. The NO_2 concentrations are similar, although the MCM predicted concentrations are slightly higher at night time at urban locations where the NO_2 concentrations are high. The predicted hydroxyl radical (OH) concentrations are slightly different between the two mechanisms. The MCM constantly predicts lower peak hour OH concentrations at all sites during the day. The two mechanisms are significantly different in the treatment of isoprene reactions but the reaction rate constants of initial OH, O_3 and NO_3 reactions with isoprene in the two models are almost identical. Thus the lower isoprene concentrations predicted by the MCM, especially during the day, are likely due to higher O_3 concentrations. The MCM mechanism predicts higher HCHO concentrations. The biggest difference occurs at CONR, where the concentrations predicted by the MCM are constantly higher than the SAPRC07 results by approximately 0.4-0.5 ppb.

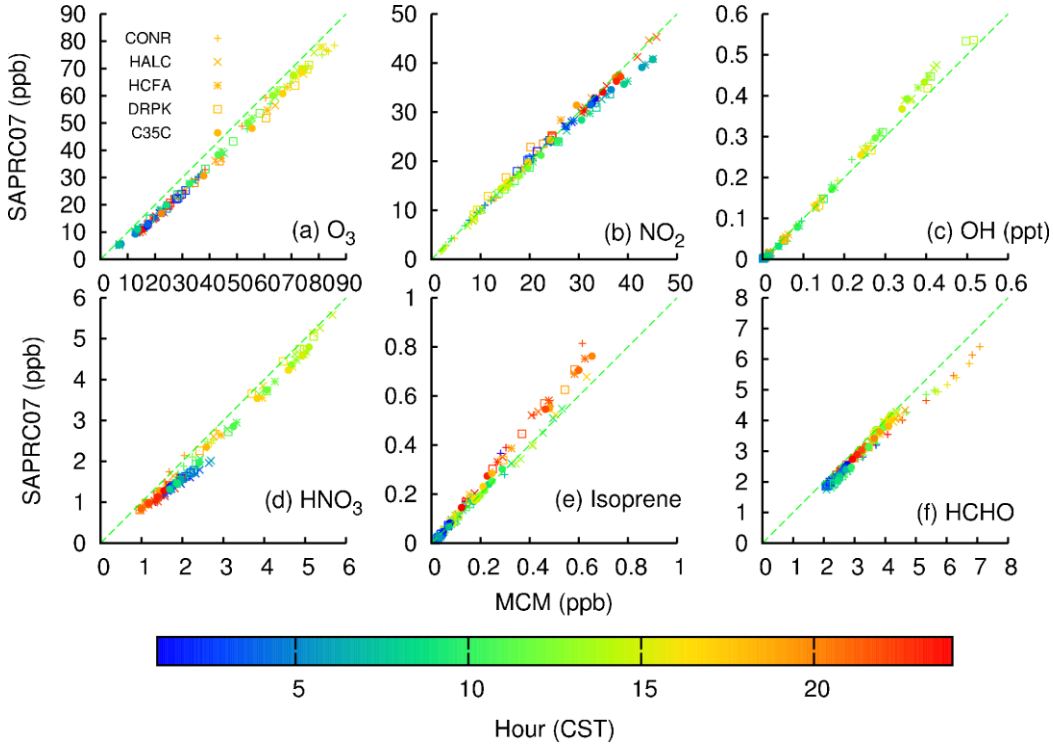

Figure 3.5 Comparison of episode-average O_3, NO_2, OH, HNO_3, isoprene and HCHO concentrations predicted by the CMAQ-MCM and CMAQ-SAPRC07 models.

Formation of O_3 and other secondary products in the atmosphere depends on the OH concentration. The lifetime of OH in the atmosphere is greatly affected by its reaction with various VOC species and the relative importance of each VOC to the OH lifetime in the atmosphere can be described by the OH reactivity. The total OH reactivity of VOCs (R_{OH}) is the sum of the products of the individual VOC species concentrations and the reaction rate coefficients with OH, as described by equation (E3.1):

$$R_{OH} = \sum_{i=1}^{N} k_{OH+VOC_i} C_{VOC,i} \qquad \text{(E3.1)}$$

where N is the total number of VOC species, $k_{OH+VOCi}$ is the reaction rate coefficient of the i^{th} VOC with OH radical and $C_{VOC,i}$ is the gas phase concentration of the i^{th} VOC species.

Figure 3.4 shows the top 10 VOC contributors to the VOC OH reactivity at CONR and C35C at 1200 CST averaged over the entire episode. The total VOC OH reactivity is 12.9 s^{-1} at CONR, which is very close to the OH reactivity predicted by the SAPRC07 mechanism of 12.4 s^{-1} (see Table 3.5 for the SARPC07 OH reactivity results). The total VOC OH reactivity is dominated by emissions from biogenic sources. C5H8 accounts for 46.3% (SAPRC07: 45.7%) of the total VOC OH reactivity and its oxidation products also contribute significantly. HCHO is the second largest contributor and accounts for approximately 9.5% (SAPRC07: 8.0%). HCHO is emitted from both anthropogenic and biogenic sources and can also be formed from oxidation reactions of isoprene with O_3. MVK is the third largest contributor (3.7%, SAPRC07: 3.4%) and is mainly emitted from biogenic sources. It could also be formed from isoprene+O_3 reaction. MACR is not emitted in significant quantities so isoprene+O_3 reaction is likely a significant source. Approximately 70% of the total VOC OH reactivity can be accounted for by 10 VOCs. C35C shows much more influences from anthropogenic emissions. The total VOC OH reactivity of 4.95 s^{-1} (SAPRC07: 6.18 s^{-1}) is much lower than that at CONR. HCHO (18.6%, SAPRC07: 12.5%) is the highest contributor followed by C5H8 (8.8%, SAPRC07: 7.8%) and C2H4 (5.1%, SAPRC07: 4.6%). N-butane (1.9%) and toluene (1.7%) are the highest contributing alkane and aromatic compounds to OH reactivity. The top 10 VOCs only account for half of the total VOC OH reactivity. The total VOC

OH reactivity is likely underestimated at C35C because the concentrations of the top contributing species are underestimated (see Section 3.4.2 below).

Table 3.4 Episode-average VOC OH reactivity at CONR and C35C at 1200 CST predicted by the MCM model

Conroe (CONR)			**Clinton Drive (C35C)**		
Species	**R_{OH} (s^{-1})**	**%**	**Species**	**R_{OH} (s^{-1})**	**%**
C5H8 (isoprene)	5.97	46.3	HCHO (formaldehyde)	0.92	18.6
HCHO (formaldehyde)	1.23	9.5	C5H8 (isoprene)	0.44	8.8
MVK (methyl vinyl ketone)	0.48	3.7	C2H4 (ethylene)	0.30	6.0
MACR (methacrolein)	0.36	2.8	CH3CHO (acetaldehyde)	0.25	5.1
ISOPBOOH [from isoprene+OH]	0.31	2.4	C3H6 (propylene)	0.18	3.6
HC4CCHO [from isoprene+OH]	0.25	1.9	HOCH2CHO [from 1,3-butadiene]	0.10	1.9
HOCH2CHO [from isoprene+O_3]	0.21	1.6	NBUTOL (n-butanol)	0.10	1.9
APINENE (α-pinene)	0.20	1.6	NC4H10 (n-butane)	0.09	1.9
ISOPDOOH [from isoprene+OH]	0.19	1.5	MVK (methyl vinyl ketone)	0.09	1.8
HC4ACHO [from isoprene+OH]	0.18	1.4	TOLUENE (toluene)	0.08	1.7
Other	3.51	27.2	Other	2.41	48.6
Total*	**12.90**	**100.0**		**4.95**	**100.0**

* OH reactions with CO and CH4 are not included in the calculation of total VOC OH reactivity.

Table 3.5 Episode averaged VOC OH reactivity at CONR and C35C at 1200 CST predicted by the SAPRC07 mechanism. Units for R_{OH} are s^{-1}

CONR				C35C			
Species	**Name**	**R_{OH} (s^{-1})**	**%**	**Species**	**Name**	**R_{OH} (s^{-1})**	**%**
ISOP	Isoprene	5.67	45.7	HCHO	formaldehyde	0.77	12.5
HCHO	Formaldehyde	0.99	8.0	CCHO	acetaldehyde	0.60	9.8
IPRD	lumped isoprene products	0.82	6.6	RCHO	higher aldehydes	0.50	8.1
PRD2	see 1	0.64	5.2	ISOP	isoprene	0.48	7.8
RCHO	higher aldehydes	0.60	4.9	OLE2	see 3	0.48	7.7
CCHO	Acetaldehyde	0.51	4.1	OLE1	see 4	0.44	7.1
R6OOH	see 2	0.51	4.1	PRD2	see 1	0.39	6.3
MVK	methyl vinyl ketone	0.42	3.4	ALK5	see 5	0.32	5.2
MACR	Methacrolein	0.42	3.4	ETHE	Ethylene	0.28	4.6
TERP	Terpenes	0.38	3.0	ARO2	see 6	0.28	4.6
Other		1.46	11.7			1.62	26.3
Total		**12.43**	**100.0**			**6.18**	**100.0**

1.* Ketones and other non-aldehyde oxygenated products that react with OH radicals faster than 5 x 10-12 cm3 molec-2 sec-1.
2. Lumped organic hydroperoxides with 5 or more carbons (other than those formed following OH addition to aromatic rings, which are represented separately).
3. Alkenes (other than ethene) with kOH < 7x104 ppm-1 min-1.
4. Alkenes with kOH > 7x104 ppm-1 min-1.
5. Alkanes and other non-aromatic compounds that react only with OH, and have kOH greater than 1 x 104 ppm-1 min-1.
6. Aromatics with kOH > 2x104 ppm-1 min-1.
*Items1-6 are taken from Carter (2010).

3.3.2 Analysis of hourly VOC concentrations at Clinton Drive and La Porte

3.3.2.1 Clinton Drive Site (C35C)

C35C is an industrial site 10 km to the west of urban Houston area and approximately 700 m to a busy freeway. Figure 3.6 shows the diurnal variation of 40 of the 46 VOC species at the C35C site based on observed and predicted median

concentrations throughout the entire modeling episode for each hour. Formaldehyde, acetaldehyde and acetone do not have enough data points so they are not included in the analysis. N-propylbenzene, iso-propylbenzene and p-ethylbenzene are not included because their concentrations are small and their diurnal variations are very similar to most of the aromatic compounds.

A large number of species show two observed peaks (for example, isopentane (b1), tolulene (g1), xylene isomers (g2 and g3), ethylbenzene (g5), trimethylbenzene isomers (h1-h3) and ethyltoluene isomers (h3-h5)). One peak occurs at 0600-0700 CST and the other peak occurs in the afternoon approximately between 18:00-21:00 CST. The morning peaks are generally well predicted by the MCM model. The good agreement with observations for most of the VOCs and CO (Figure 3.7(a)) in the morning suggests that exhaust emissions from mobile sources and upwind urban sources are likely well represented in the emission inventory, as the wind in the morning hours is generally from the west during this episode (Figure 3.8(a,c)).

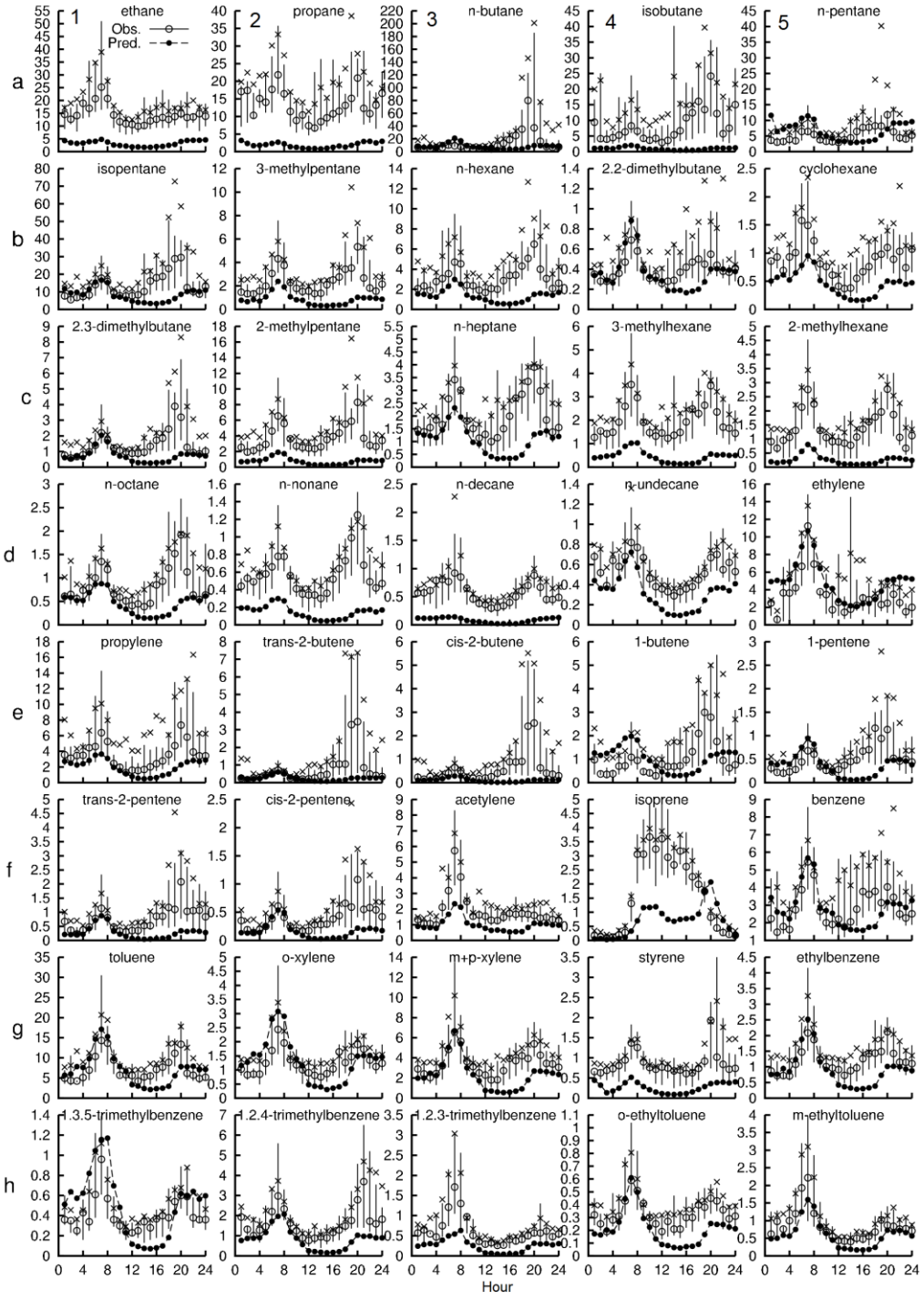

Figure 3.6 Median concentrations of VOCs at the Clinton Drive (C35C) from August 18 to September 6, 2000. The bars are the range of 25-75th percentiles. The × symbols show episode

average of the observed concentrations. The rows are indexed by letters a-h and the columns by numbers 1-5. Units are ppbC.

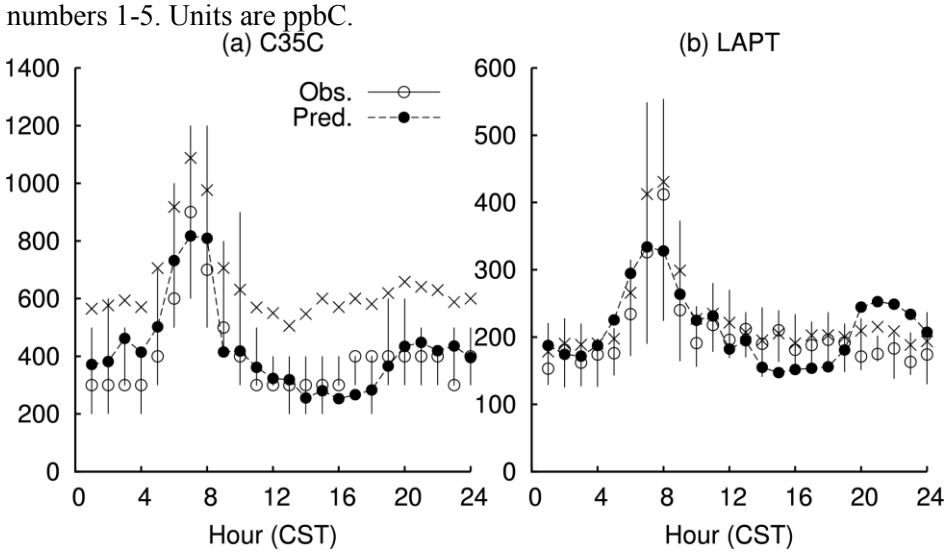

Figure 3.7 Median concentrations of CO at C35C and LAPT from August 18 to September 6, 2000. The bars show 25-75th percentile of the observations. The × symbol denotes episode average of observed concentrations. Units are ppb**.**

The increases of a large number of VOCs in the afternoon are not predicted by the MCM model. Diurnal variations of predicted and observed CO at C35C and LAPT (Figure 3.7) show only slight increase of the concentrations in the evening, suggesting that the large under-predictions in the afternoon concentrations are not due to underestimation of vehicle exhaust emissions. Frequency distributions of the wind speed and direction measured and predicted at C35C show that wind is dominantly from the west between 0500-1200 CST (Figure 3.8(a,c)) but switches to south-southeast where most of the industrial sources are located between 1300-2100 CST (Figure 3.8(b,d)). This suggests that the missing sources of VOCs in the afternoon are likely located in the industrial areas to the south of C35C. The emission rates of the compounds have to increase in the afternoon in order to overcome the dilution effect due to the growth of the

convective mixing layer to allow continued increase of the concentrations. The missing emissions are likely from evaporative sources, as the ambient temperature could increases to more than 38^{o}C in the afternoon (Figure 3.9). However, detailed source apportionment studies are needed to correctly attribute the observed concentrations to their respective sources and identify missing sources in the emission inventory.

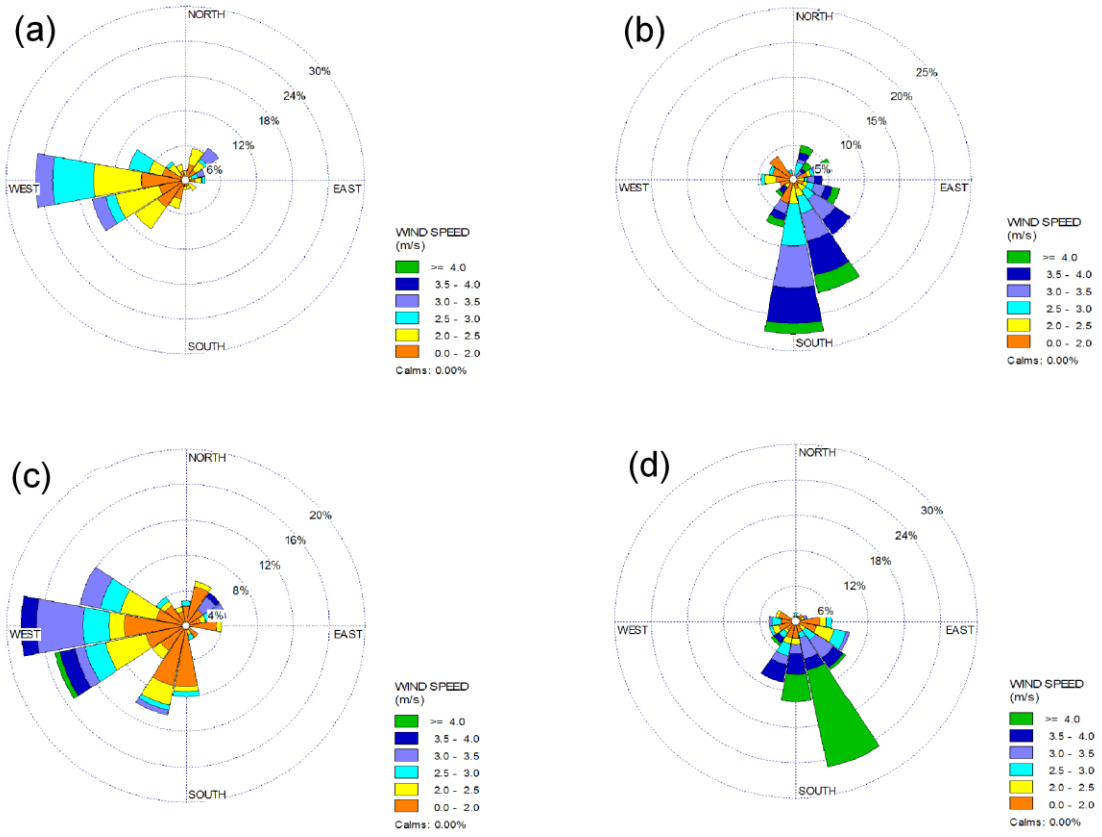

Figure 3.8 Predicted (a,b) and observed (c,d) distributions of wind speed and wind direction at C35C in the morning (a,c) (5:00-12:00 CST) and afternoon (b,d) (13:00-21:00 CST) on August 18 – September 6, 2000.

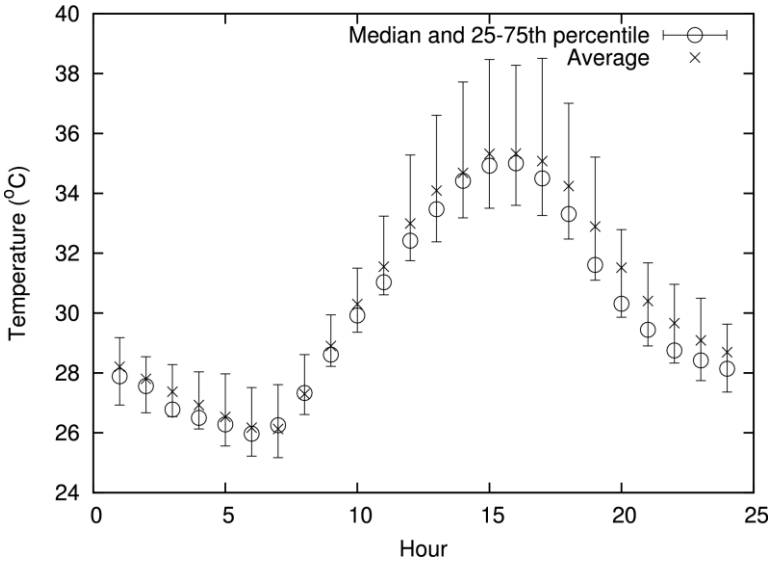

Figure 3.9 Median and mean temperature at C35C.

Some other species, such as acetylene (f3) and 1,2,3-trimethylbenzene (h3), show a much significant morning peak but no prominent afternoon peak. The concentrations of these species are significantly under-predicted by the MCM model. This suggests that the emissions of these compounds from upwind sources such as vehicles are likely underestimated. Since the detailed emissions of these compounds are based on the speciation profiles and the overall VOC emission rates, the fraction of these compounds in the speciation profiles might be too low.

Some species, such as n-butane (a3) and 2-butenes (e2-3), show a large increase in the median concentrations in the afternoon at 18:00-19:00 CST superimposed on the general afternoon increase tread. The large difference in the mean and median concentrations and wide range of the 25-75th percentiles are due to large transient emissions that occur on a few days during the episode. The similar timing of these events

implies that they are possibly coming from the same industrial sources. Since these transient emissions are not properly accounted for in the current emission inventory, the MCM predicted concentrations are much lower.

The predicted concentrations of ethane (a1), propane (a2), isobutane (a4), methylhexanes (c4 and c5), propylene (e1) and styrene (g4) are significantly lower than observations at all hours. Major sources of ethane, propane, propylene, isobutene, styrene are refinery and petrochemical industries (Buzcu and Fraser, 2006; Zhao et al., 2004). However, dominant wind from west in the morning suggests that sources which can emit large amount of small alkanes (such as natural gas combustions) in the urban areas are also missing or significantly underestimated when reporting total VOC emissions. Isoprene (f4) concentrations are low at night but increase rapidly when the sun comes up. Highest concentrations occur at noon but are under-predicted by the MCM, likely due to missing biogenic emissions.

3.3.2.2 La Porte Airport site (LAPT)

Figure 3.10 shows the diurnal variation of the hourly predicted and observed median concentrations of 32 VOCs at the La Porte Airport site (LAPT, see Figure 3.1). Industrial facilities are in the north, northeast, northwest, south and southwest directions within 4-10 km of the LAPT site. Similar to C35C, wind is mainly from the west during morning hours and switch to south-southeast in the afternoon and evening hours (Figure 3.11). The VOC concentrations were measured by gas chromatography with a flame ionization detector (GC-FID) and a quadrupole ion trap mass spectrometer detector (GC-ITMS),

both operated by the National Oceanic and Atmospheric Administration's Aeronomy Laboratory (Kuster et al., 2004). In this analysis, concentrations of ethane, propane, n-butane, 2.2-dimethylbutane, ethylene, trans-2-butene, propylene, 1-butene, acetylene, and cis-2-butene are based on GC-FID measurements and other species are based on GC-ITMS measurements.

The observed diurnal variations of VOCs at LAPT are significantly different from those measured at C35C. A significant morning peak still exists for most of the VOC species but there lacks significant afternoon peaks. The predicted concentrations of CO (Figure 3.7(b)) agree well with observations although the morning peaks are slightly under-predicted. Similarity of the CO and VOC diurnal profiles indicate that this area is likely influenced significantly by vehicle emissions. The morning peaks of 3-methylpentane (a5), n-hexane (b1), cyclohexane (b3), and 2-methylpentane (b4) are significantly under-predicted, similar to predictions at C35C. Most of the C2-C5 alkenes (c2-d4), n-butane (a3) and n-pentane (a4) show large ranges of the 25-75% quartiles and significant differences in the mean and median concentrations in the morning hours. This suggests that some industrial sources to the west of LAPT are likely to have transient emission events in the morning hours.

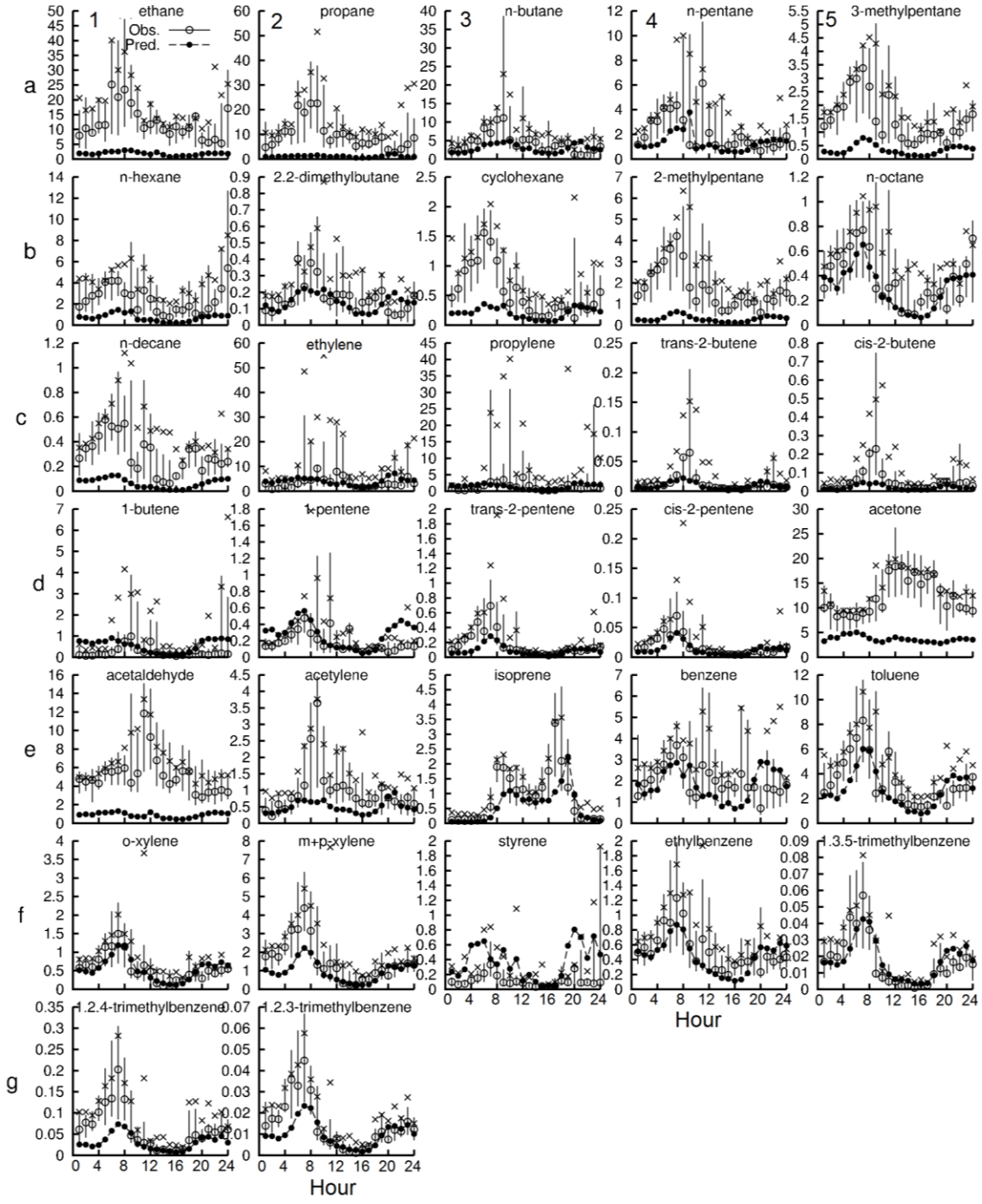

Figure 3.10 Same as Figure 7 but for La Porte Airport (LAPT). Units are ppbC.

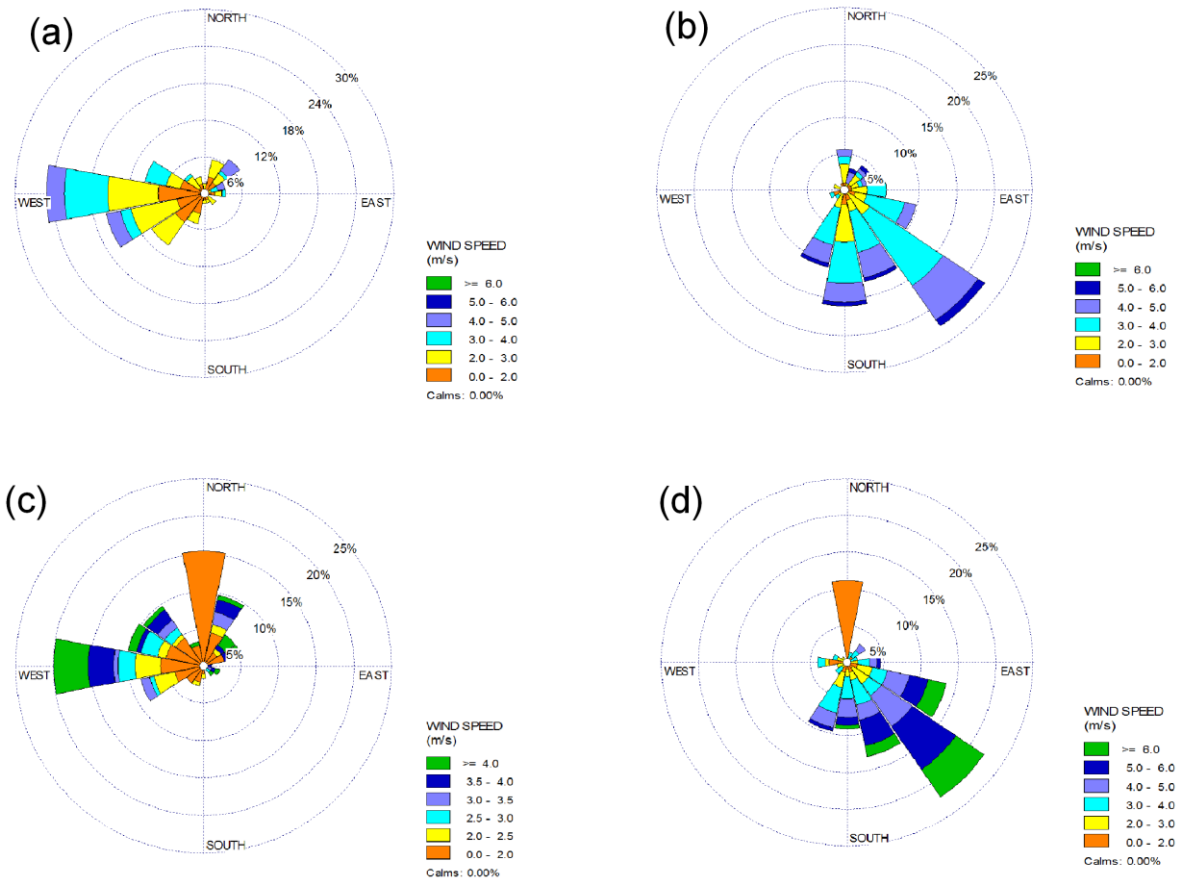

Figure 3.11 Predicted (a,b) and observed (c,d) distributions of wind speed and wind direction at LAPT in the morning (a,c) (0500-1200 CST) and afternoon (b,d) (1300-2100 CST) on August 18 – September 6, 2000.

Acetone (d5) concentrations are high throughout the day, with ~10 ppbC in the early morning and nighttime hours and ~20 ppbC during the day with peak concentrations occur at noon time. The predicted acetone concentrations are significantly lower by a factor of 2-4 and without significant diurnal variations. Both natural source (direct emissions from vegetation and oxidation of monoterpenes) and anthropogenic sources

(mainly oxidation of small isoalkanes such as propane) could contribute to acetone concentrations (Jacob et al., 2002). Since the propane concentrations are significantly under-predicted in the current simulation, it is likely that this is also the main cause of acetone under-prediction. Similarly, acetaldehyde (e1) is also under-predicted, likely due to under-prediction of parent VOCs. The observed isoprene (e3) shows a clear diurnal variation with two peaks, one in the morning (0800-0900 CST) and one in the afternoon (16:00-18:00 CST). The MCM predictions generally agree with observations with slight under-predictions, likely due to underestimation of anthropogenic isoprene (Song et al., 2008). The predicted aromatic compound concentrations (e4-g2) agree better with observations than other groups of compounds. Although the morning concentrations are under-predicted, the afternoon and night time concentrations agree well with observations.

3.3.3 Analysis of regional VOC concentrations

In addition to C35C and LAPT, 24-hr average VOC samples were collected by canister samplers every 6 days during this episode at 24 stations (open circles in Figure 3.1(b)). These data provide wider spatial coverage for a more complete regional evaluation of the MCM model predictions. Figure 3.12 shows the comparison of the predicted and observed 24-hr VOC concentrations. The model performance evaluation is based on the mean fractional bias (MFB), as defined in equation (E3.2):

$$MFB = \frac{2}{N}\sum_{i=1}^{N}\left(\frac{P_i - O_i}{O_i + P_i}\right) \quad \text{(E3.2)}$$

where N is the number of data points. P and O denote predicted and observed concentrations, respectively. However, MFB ranges from -2 to 2 and varies non-linearly as the prediction deviates from the observation, which is not very intuitive in describing the model performance. The ratio of observation to prediction (O/P ratio) based on MFB, as defined in equation (E3.3), can provide a more intuitive description of the difference between the observations and predictions:

$$\frac{O}{P} = \frac{2 - MFB}{2 + MFB} \quad \text{(E3.3)}$$

The other advantage of the O/P ratio is that it can be directly used as a first order approximation to adjust emissions of individual species in the emission inventory. Thus, instead of MFB, the O/P ratio of each species is show on Figure 3.12. Alkane concentrations (a1-d4) are under-predicted at all stations. Ethane (a1), propane (a2), isobutane (a4) and 2-methylpentane (c2) are under-predicted by a factor of 6.0-16.8. Other alkanes are generally under-predicted by a factor of 2-5. Although the alkane species do not contribute much to the peak O_3 formation due to their slower reaction rates with OH, the large C8-C12 alkanes can be oxidized to form low volatile species thus affect SOA predictions (Jordan et al., 2008). Ethylene (d5) concentrations are under-predicted by a factor of 2 on average but could be under-predicted by a factor of 5

or more. The concentrations of propylene and other alkenes are more severely under-predicted by approximately a factor of 2-5. Predicted concentrations of aromatic species (f5-h5) agree better with observations than other alkanes and aromatics. Benzene (f5) and styrene (g5) are under-predicted by a factor of 1.8 and 3.5 on average, respectively. Toluene, xylenes and other aromatic compounds show no significant biases in the predicted concentrations with O/P ratio ranges from 0.9-1.5. Isoprene concentrations are under-predicted by approximately 50%.

3.3.4 Computation time

The simulation for the 4 km domain was carried out using 30 computer nodes equipped with one Intel Q6600 processor per node. Only one out of the four available CPU cores in each Q6600 was used in the simulation. The nodes are interconnected with Gigabit Ethernet. On average, each time step (typically 4-6 min) takes 235.1s (wall clock time) to complete. The most time consuming part is horizontal advection, which takes 57% of the time. Chemistry takes 32% of the time and 10% of the time is spent on data input/output (I/O), which includes the waiting time of the master node for other nodes to complete after a chemistry step due to load imbalance. Only 1.5% of the time is spent on diffusion and vertical advection processes combined.

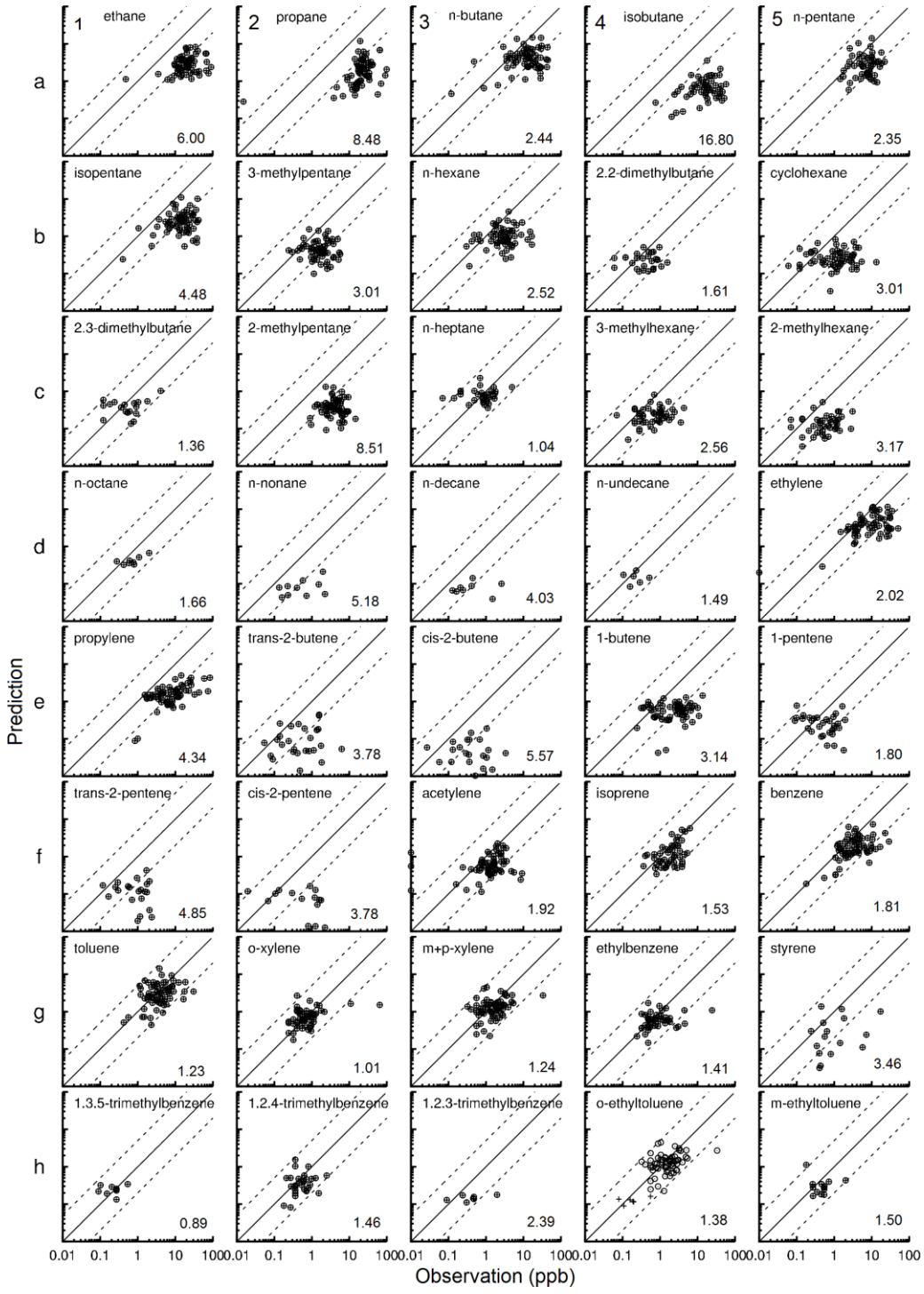

Figure 3.12 Predicted vs. observed 24-hr average VOC concentrations from August 18 to September 6, 2000. Solid line represents 1:1 ratio and two dashed lines represent 1:5 and 5:1 ratios. The numbers on the lower right corner is the O/P ratio (see text for details).

Using more nodes will reduce the amount of time spent in chemistry but not necessary in horizontal advection calculations where concentrations of species have to be passed to adjacent nodes. To test the scalability of CMAQ in handling horizontal transport, the model was modified to include a dummy mechanism that contains 5000 non-reactive species. As illustrated in Figure 3.13, the CMAQ can simulate the transport of the 5000 species in approximately 4 minutes per time step for an 85x83x15 domain with 12 km grid resolution. Increasing the number of nodes does not significantly reduce the transport time when the number of nodes exceeds 15 in our system.

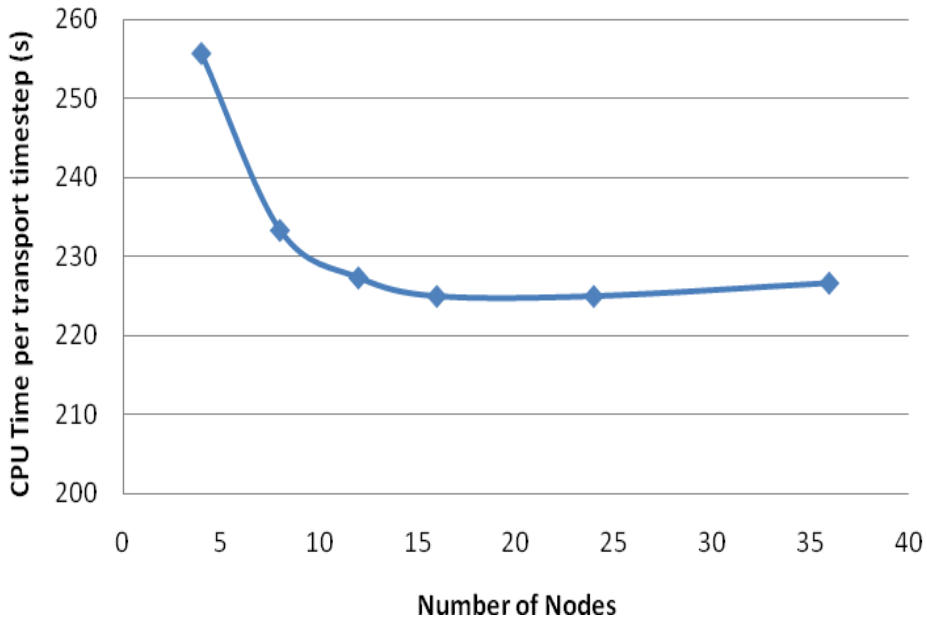

Figure 3.13 Time needed for the horizontal advection of 5000 species for one time step as a function of number of nodes used in the computer cluster. The tests use the 12 km horizontal resolution domain with 85x83x15 grid cells.

3.4 Conclusions

In this study, a modified MCM with 4642 species and 13566 reactions was incorporated into the CMAQ model. The model successfully reproduced the observed O_3 concentrations throughout the Southeast Texas region during TexAQS 2000, with model performance similar to that of the expanded standard SAPRC07. The MCM predicted slightly higher O_3 concentrations but lower OH concentrations. The MCM predicted VOC OH reactivity is similar to the SAPRC07 predictions at CONR where biogenic emissions dominate the OH reactivity and is slightly lower than SAPRC07 predictions at C35C where anthropogenic emissions dominate.

The CMAQ-MCM has been demonstrated to be a useful tool to evaluate the emission inventory of VOCs by directly predicting the concentrations of large number of detailed VOC species. The predicted 1-hr average concentrations of major O_3 precursor VOC species at C35C, LAPT and 24-hr average concentrations at other stations show universal underestimation of most of the alkane and alkene concentrations by a factor 2-5. The under-prediction of ethane and propane is more significant, by a factor of 6 and 8, respectively. Major aromatic compounds generally agree better with observation. Benzene is under-predicted by approximately 80%. Species specific emission adjustment factors based on the O/R ratio can be derived from these direct comparisons to improve emission inventories in future studies. Most of the under-predictions at C35C happen in the afternoon when industrial facilities are in the immediate upwind direction and the missing industrial emissions are likely evaporative sources whose emission rates are temperature dependent. VOC concentrations at LAPT are lower and show similar diurnal

variation as CO. Emissions from transient events typically arrive at LAPT from the west in the morning hours. The CMAQ-MCM can be used on small clusters with slow interconnections and the most time consuming part is the horizontal advection process, which takes approximately 60% of the computation time.

4. CONCLUSIONS

Two different photolysis mechanisms, expanded standard SAPRC07 and modified MCM v3.1 have been implemented in the 3D Community Multi-scale Air Quality (CMAQ) model and model performances are evaluated by comparing the predictions to observations and predictions of an different photolysis mechanism in each case. SAPRC99 predicts higher ozone concentration than SAPRC07 by a maximum difference about 20%. SAPRC07 presents big differences in predictions of OH, PAN, HCHO, and HNO_3, compared to SAPRC99 results, which are due to the updated reaction rates, updated treatment of VOC reactions and new added reactions and species in SAPRC07. Process analysis of ozone mechanism in SAPRC07 and SAPRC99 indicates that difference in the new generated OH rates of $O(^1D)$ (from photolysis of O_3) and H_2O is one of the major reaction that SAPRC07 predicts lower ozone concentration than SAPRC99. The ozone relative response factor (RRF) predicted by the two mechanisms are very similar, suggesting that SAPRC07 can be used to replace with SAPRC99 in regulatory modeling without causing much changes.

The MCM mechanism is much complex photochemical mechanism to implement in 3D air quality models due to its large number of species and near-explicit treatment of the VOC reactions. Results of SAPRC07 and MCM are quite similar, and MCM also has a good consistent with the observation data according to statistical analysis results at several stations in the 4km simulation domain. VOC OH reactivity predicted by MCM and SAPRC07 is different in the area where anthropogenic emissions dominate, but quite similar in rural area. The MCM is very useful in evaluating emission inventory.

Comparison of 1hr and 24hr prediction of major O_3 precursor VOCs to the observation data indicates that alkanes, alkenes, ethane, propane and benzene are under predicted. Missed sources of emission at C35C in the afternoon are likely temperature dependent, such as evaporation of gasoline and solvents. Future development of the MCM mechanism will be focused on its ability to predict detailed SOA compositions.

REFERENCES

Azzi, M., S. White and D. Angove, 2008. Review of the SAPRC-07 chemical mechanism. Report to the California Air Resources Board, November.

Bloss, C., Wagner, V., Jenkin, M.E., Volkamer, R., Bloss, W.J., Lee, J.D., Heard, D.E., Wirtz, K., Martin-Reviejo, M., Rea, G., Wenger, J.C., Pilling, M.J., 2005. Development of a detailed chemical mechanism (MCMv3.1) for the atmospheric oxidation of aromatic hydrocarbons. Atmospheric Chemistry and Physics, 5, 641-664.

Brown, S.G., Reid, S.B., Roberts, P.T., Buhr, M.P., Funk, T.H., Kim, E., Hopke, P.K., 2004. Reconciliation of the VOC and NO_x emission inventory with ambient data in the Houston, Texas Region. 13th International Emission Inventory Conference, Working for Clean Air in Clearwater, Clearwater, Florida.

Buzcu, B., Fraser, M.P., 2006. Source identification and apportionment of volatile organic compounds in Houston, Texas. Atmospheric Environment, 40, 2385-2400.

Buzcu-Guven, B., Fraser, M.P., 2008. Comparison of VOC emissions inventory data with source apportionment results for Houston, Texas. Atmospheric Environment, 42, 5032-5043.

Byun, D.W., 2002. A study of photochemical processes of the Houston-Galveston metropolitan airshed with EPA CMAQ. Available at http://www.cmascenter.org/ conference/2002/session4/byun_abstract.pdf. Accessed on 10/07/2010

Byun, D.W., Kim, S.T., Kim, S.B., 2007. Evaluation of air quality models for the simulation of a high ozone episode in the Houston metropolitan area. Atmospheric Environment, 41, 837-853.

Byun, D.W., Schere, K.L., 2006. Review of the governing equations, computational algorithms and other components of the Models-3 Community Multi-scale Air Quality (CMAQ) modeling system. Applied Mechanics Review, 59, 51-78.

Cai, C.X., Kelly, J.T., Avise, J.C., Kaduwela, A.P., Stockwell, W.R., 2010. Implementation of the SAPRC07C chemical mechanism in the Community Multi-scale Air Quality (CMAQ) model for photochemical modeling in California: Comparisons with SAPRC99, in preparation.

Carslaw, N., Creasey, D.J., Heard, D.E., Lewis, A.C., McQuaid, J.B., Pilling, M.J., Monks, P.S., Bandy, B.J., Penkett, S.A., 1999. Modeling OH, HO_2, and RO_2 radicals

in the marine boundary layer - 1. Model construction and comparison with field measurements. Journal of Geophysical Research-Atmospheres, 104, 30241-30255.

Carter, W.P.L., 1990. A detailed mechanism for the gas-phase atmospheric reactions of organic compounds. Atmospheric Environment Part A - General Topics 24, 481-518.

Carter, W.P.L., 1994. Development of ozone reactivity scales for volatile organic-compounds. Journal of the Air & Waste Management Association, 44, 881-899.

Carter, W.P.L., 2000. Documentation of the SAPRC-99 chemical mechanism for VOC reactivity assessment, report to the California Air Resources Board. Available at http://cert.ucr.edu/~carter/absts.htm#saprc99 and http://www.cert.ucr.edu /~carter/reactdat.htm. Accessed on 10/05/2010

Carter, W.P.L., 2004. Development of a chemical speciation database and software for processing VOC emissions for air quality models, Proc. of the 13th International Emission Inventory Conference, Working for Clean Air in Clearwater, Clearwater, Florida.

Carter, W.P.L., 2010. Development of the SAPRC-07 chemical mechanism. Atmospheric Environment, in press, corrected proof.

Czader, B.H., Byun, D.W., Kim, S.T., Carter, W.P.L., 2008. A study of VOC reactivity in the Houston-Galveston air mixture utilizing an extended version of SAPRC-99 chemical mechanism. Atmospheric Environment, 42, 5733-5742.

Derwent, R.G., Jenkin, M.E., and Pilling, M.J., 2008. Reactivity scales as comparative tools for chemical mechanisms: SAPRC vs. MCM. Final Report to the California Air Resources Board.

Dodge, M.C., 2000. Chemical oxidant mechanisms for air quality modeling: Critical review. Atmospheric Environment, 34, 2103-2130.

Emmerson, K.M., MacKenzie, A.R., Owen, S.M., Evans, M.J., Shallcross, D.E., 2004. A Lagrangian model with simple primary and secondary aerosol scheme 1: Comparison with UK PM10 data. Atmospheric Chemistry and Physics, 4: 2161-2170.

EPA, 2004. Region 6: State designations for the 1997 8-hour ozone standard. Available at http://www.epa.gov/ozonedesignations/1997standards/regions/region6desig.htm. Accessed on 10/07/2010.

EPA, 2007. Guidance on the use of models and other analyses for demonstrating attainment of air quality goals for O_3, PM2.5 and regional haze. In Agency, U.S.E.P. (Ed.), Research Triangle Park, North Carolina.

Faraji, M., Kimura, Y., McDonald-Buller, E., Allen, D., 2008. Comparison of the carbon bond and SAPRC photochemical mechanisms under conditions relevant to southeast Texas. Atmospheric Environment, 42, 5821-5836.

Fraser, M.P., Kleeman, M.J., Schauer, J.J., Cass, G.R., 2000. Modeling the atmospheric concentrations of individual gas-phase and particle-phase organic compounds. Environmental Science & Technology, 34, 1302-1312.

Gery, M.W., Whitten, G.Z., Killus, J.P., Dodge, M.C., 1989. A photochemical kinetics mechanism for urban and regional scale computer modeling. Journal of Geophysical Research-Atmospheres, 94, 12925-12956.

Griffin, R.J., Dabdub, D., Seinfeld, J.H., 2005. Development and initial evaluation of a dynamic species-resolved model for gas phase chemistry and size-resolved gas/particle partitioning associated with secondary organic aerosol formation. Journal of Geophysical Research-Atmospheres, 110 (D05304).

Harley, R.A., Cass, G.R., 1995. Modeling the atmospheric concentrations of individual volatile organic-compounds. Atmospheric Environment, 29, 905-922.

Henry, R.C., Lewis, C.W., Collins, J.F., 1994. Vehicle-related hydrocarbon source compositions from ambient data - the grace-safer method. Environmental Science & Technology, 28, 823-832.

Jacob, D.J., Field, B.D., Bey, E.J.I., Li, Q., Jennifer A. Logan, Yantosca, R.M., 2002. Atmospheric budget of acetone. Journal of Geophysical Research-Atmospheres, 107 (D10).

Jacobson, M.Z., Ginnebaugh, D.L., 2010. Global-through-urban nested three-dimensional simulation of air pollution with a 13,600-reaction photochemical mechanism. Journal of Geophysical Research-Atmospheres 115 (D14304).

Jacobson, M.Z., Turco, R.P., 1994. SMVGEAR: A sparse-matrix, vectorized gear code for atmospheric models. Atmospheric Environment, 28, 273-284.

Jang, J.-C.C., Jeffries, H.E., Tonnesen, S., 1995. Sensitivity of ozone to model grid resolution -- II: Detailed process analysis for ozone chemistry. Atmospheric Environment, 29, 3101-3114.

Jenkin, M.E., Saunders, S.M., Pilling, M.J., 1997. The tropospheric degradation of volatile organic compounds: A protocol for mechanism development. Atmospheric Environment, 31, 81-104.

Jenkin, M.E., Saunders, S.M., Wagner, V., Pilling, M.J., 2003. Protocol for the development of the Master Chemical Mechanism, MCM v3 (Part B): Tropospheric degradation of aromatic volatile organic compounds. Atmospheric Chemistry and Physics, 3, 181-193.

Jimenez, P., Baldasano, J.M., Dabdub, D., 2003. Comparison of photochemical mechanisms for air quality modeling. Atmospheric Environment, 37, 4179-4194.

Johnson, D., Jenkin, M.E., Wirtz, K., Martin-Reviejo, M., 2004. Simulating the formation of secondary organic aerosol from the photooxidation of toluene. Environmental Chemistry, 1, 150-165.

Johnson, D., Jenkin, M.E., Wirtz, K., Martin-Reviejo, M., 2005. Simulating the formation of secondary organic aerosol from the photooxidation of aromatic hydrocarbons. Environmental Chemistry, 2, 35-48.

Johnson, D., Utembe, S.R., Jenkin, M.E., 2006a. Simulating the detailed chemical composition of secondary organic aerosol formed on a regional scale during the TORCH 2003 campaign in the southern UK. Atmospheric Chemistry and Physics, 6, 419-431.

Johnson, D., Utembe, S.R., Jenkin, M.E., Derwent, R.G., Hayman, G.D., Alfarra, M.R., Coe, H., McFiggans, G., 2006b. Simulating regional scale secondary organic aerosol formation during the TORCH 2003 campaign in the southern UK. Atmospheric Chemistry and Physics, 6, 403-418.

Jordan, C.E., Ziemann, P.J., Griffin, R.J., Lim, Y.B., Atkinson, R., Arey, J., 2008. Modeling SOA formation from OH reactions with C-8-C-17 n-alkanes. Atmospheric Environment, 42, 8015-8026.

Kuster, W.C., Jobson, B.T., Karl, T., Riemer, D., Apel, E., Goldan, P.D., Fehsenfeld, F.C., 2004. Intercomparison of volatile organic carbon measurement techniques and data at la porte during the TexAQS2000 Air Quality Study. Environmental Science & Technology, 38, 221-228.

Liang, J.Y., Jacobson, M.Z., 2000. Comparison of a 4000-reaction chemical mechanism with the carbon bond IV and an adjusted carbon bond IV-EX mechanism using SMVGEAR II. Atmospheric Environment, 34, 3015-3026.

NRC, 1991. Rethinking the ozone problem in urban and regional air pollution. National Research Council Committee on Tropospheric Ozone Formation and Measurement. National Academy Press, Washington D.C..

Pinho, P.G., Pio, C.A., Carter, W.P.L., Jenkin, M.E., 2006. Evaluation of alkene degradation in the detailed tropospheric chemistry mechanism, MCM v3, using environmental chamber data. Journal of Atmospheric Chemistry, 55, 55-79.

Pinho, P.G., Pio, C.A., Carter, W.P.L., Jenkin, M.E., 2007. Evaluation of alpha- and beta-pinene degradation in the detailed tropospheric chemistry mechanism, MCM v3.1, using environmental chamber data. Journal of Atmospheric Chemistry, 57, 171-202.

Pinho, P.G., Pio, C.A., Jenkin, M.E., 2005. Evaluation of isoprene degradation in the detailed tropospheric chemical mechanism, MCM v3, using environmental chamber data. Atmospheric Environment, 39, 1303-1322.

Saunders, S.M., Jenkin, M.E., Derwent, R.G., Pilling, M.J., 2003. Protocol for the development of the Master Chemical Mechanism, MCM v3 (Part A): tropospheric degradation of non-aromatic volatile organic compounds. Atmospheric Chemistry and Physics, 3, 161-180.

Song, J., Vizuete, W., Chang, S., Allen, D., Kimura, Y., Kemball-Cook, S., Yarwood, G., Kioumourtzoglou, M.-A., Atlas, E., Hansel, A., Wisthaler, A., McDonald-Buller, E., 2008. Comparisons of modeled and observed isoprene concentrations in southeast Texas. Atmospheric Environment, 42, 1922-1940.

Stockwell, W.R., 2009. Peer review of the SAPRC-07 chemical mechanism of Dr. William Carter. Draft report to the California Air Resources Board. Available at http://www.arb.ca.gov/research/reactivity/rsac.htm.Accessed on 10/07/2010.

Stockwell, W.R., Kirchner, F., Kuhn, M., Seefeld, S., 1997. A new mechanism for regional atmospheric chemistry modeling. Journal of Geophysical Research-Atmospheres, 102, 25847-25879.

TCEQ, 2002. Conceptual model for ozone formation in the Houston-Galveston Area. Appendix A to Phase I of the mid course review modeling protocol and technical support document. Texas Commission of Environmental Quality, Texas.

TexAQS 2000. Availabel at http://www.utexas.edu/research/ceer/texaqs/participants/about.html. Accessed on 10/07/2010.

Vukovich, J.M., Pierce, T., 2002. The Implementation of BEIS3 within the SMOKE modeling framework. MCNC-Environmental Modeling Center, Research Triangle Park, North Carolina, and National Oceanic and Atmospheric Administration, Maryland.

Watson, J.G., Chow, J.C., Fujita, E.M., 2001. Review of volatile organic compound source apportionment by chemical mass balance. Atmospheric Environment, 35, 1567-1584.

Yarwood, G., Rao, S., Yocke, M., Whitten, G.Z., 2005. Updates to the carbon bond chemical mechanism: CB05. Final report to the U.S. EPA, RT-0400675. Available at www.camx.com. Accessed on 10/07/2010.

Ying, Q., Fraser, M.P., Griffin, R.J., Chen, J.J., Kleeman, M.J., 2007. Verification of a source-oriented externally mixed air quality model during a severe photochemical smog episode. Atmospheric Environment, 41, 1521-1538.

Ying, Q., Krishnan, A., 2010. Source contributions of volatile organic compounds to ozone formation in southeast Texas. Journal of Geophysical Research-Atmospheres Accepted for publication.

Zhao, W., Hopke, P.K., Karl, T., 2004. Source identification of volatile organic compounds in Houston Texas. Environmental Science & Technology, 38, 1338-1347.

VITA

Name:	Jingyi Li
Address:	WERC 204, 3136 TAMU, College Station, TX 77840-3136
Email Address:	Jingyi_li152@hotmail.com
Education:	B.S., Environmental Science, Tianjin University, China 2004 M.S., Civil Engineering, Texas A&M University, 2010